Received: 17 December 2023 | Revised: 29 February 2024 | Accepted: 8 March 2024

DOI: 10.1002/alz.13819

Alzheimer's & Dementia®
THE JOURNAL OF THE ALZHEIMER'S ASSOCIATION

RESEARCH ARTICLE

Progressive reduction of nuclear receptor Nr4a1 mediates age-dependent cognitive decline

Jiang Chen[1,2,3,4] | Zhi Zhang[1,2,3,4] | Ying Liu[1,2,3,4] | Lili Huang[1,2,3,4] | Yi Liu[1,2,3,4] | Dan Yang[1,2,3,4] | Xinyu Bao[1,2,3,4] | Pinyi Liu[1,2,3,4] | Yuhan Ge[1,2,5] | Qingqing Li[1,2,5] | Xin Shu[1,2,3,4] | Lushan Xu[1,2,3,4] | Yun Stone Shi[1,2,5] | Xiaolei Zhu[1,2,3,4] | Yun Xu[1,2,3,4]

[1]Department of Neurology, Nanjing Drum Tower Hospital, Affiliated Hospital of Medical School, Nanjing University, Nanjing, China

[2]State Key Laboratory of Pharmaceutical Biotechnology and Institute of Translational Medicine for Brain Critical Diseases, Nanjing University, Nanjing, China

[3]Jiangsu Key Laboratory for Molecular Medicine, Medical School of Nanjing University, Nanjing, China

[4]Nanjing Neurology Clinical Medical Center, Nanjing, China

[5]Ministry of Education Key Laboratory of Model Animal for Disease Study, Model Animal Research Center, Nanjing University, Nanjing, China

Correspondence
Yun Xu and Xiaolei Zhu, Department of Neurology, Nanjing Drum Tower Hospital, Affiliated Hospital of Medical School, Nanjing University, Nanjing 210008, China.
Email: xuyun20042001@aliyun.com and zhuquelee@126.com

Funding information
National Natural Science Foundation of China, Grant/Award Numbers: 81920108017, 82130036, 81630028, 81971009, 82271891, 81901161; National Science and Technology Innovation 2030 - Major Program of Brain Science and Brain-Like Researches, Grant/Award Number: 2022ZD0211800; Jiangsu Province Key Medical Discipline, Grant/Award Number: ZDXKA2016020; Natural Science Foundation of Jiangsu Province, Grant/Award Number: BK20231120; Nanjing Medical Science and Technology Development Foundation, Grant/Award Number: ZKX22025

Abstract

INTRODUCTION: Cognitive decline progresses with age, and Nr4a1 has been shown to participate in memory functions. However, the relationship between age-related Nr4a1 reduction and cognitive decline is undefined.

METHODS: Nr4a1 expressions were evaluated by quantitative PCR and immunochemical approaches. The cognition of mice was examined by multiple behavioral tests. Patch-clamp experiments were conducted to investigate the synaptic function.

RESULTS: NR4A1 in peripheral blood mononuclear cells decreased with age in humans. In the mouse brain, age-dependent Nr4a1 reduction occurred in the hippocampal CA1. Deleting Nr4a1 in CA1 pyramidal neurons (PyrNs) led to the impairment of cognition and excitatory synaptic function. Mechanistically, Nr4a1 enhanced TrkB expression via binding to its promoter. Blocking TrkB compromised the cognitive amelioration with Nr4a1-overexpression in CA1 PyrNs.

DISCUSSION: Our results elucidate the mechanism of Nr4a1-dependent TrkB regulation in cognition and synaptic function, indicating that Nr4a1 is a target for the treatment of cognitive decline.

KEYWORDS
aging, cognitive decline, Nr4a1, synaptic plasticity, TrkB

Highlights

- Nr4a1 is reduced in PBMCs and CA1 PyrNs with aging.
- Nr4a1 ablation in CA1 PyrNs impaired cognition and excitatory synaptic function.
- Nr4a1 overexpression in CA1 PyrNs ameliorated cognitive impairment of aged mice.
- Nr4a1 bound to TrkB promoter to enhance transcription.
- Blocking TrkB function compromised Nr4a1-induced cognitive improvement.

Jiang Chen and Zhi Zhang contributed equally to this study.

1 | BACKGROUND

With the sharp increase in the human life span worldwide, aging has become a growing concern. A typical sign of aging is cognitive decline, which progresses slowly with age.[1,2] In most individuals, nonpathological brain aging or normal cognitive aging occurs, which compromises the quality of daily life and social interactions. Others develop pathological cognitive impairments, such as dementia or even Alzheimer's disease (AD). Regardless of nonpathogenic or pathogenic status, age-related cognitive decline is correlated with structural and biochemical alterations in the brain.[3–5] The hippocampus is one of the key brain regions associated with learning and memory.[6,7] Strikingly, synapse structure and function in the hippocampus are particularly vulnerable to age-related changes,[8] making this brain region a focus for understanding neuronal alterations with aging and cognitive decline. Excitatory synaptic neurotransmission and plasticity in hippocampal Schaffer collateral-CA1 (SC-CA1) synapses are particularly robust models for understanding these changes in neuronal functions.[9–11]

Recently, emerging evidence has shown that nuclear receptor subfamily 4 group A (Nr4a) may play a role in cognition. This orphan receptor family in rodents contains three immediate early genes (IEGs), *Nr4a1*, *Nr4a2*, and *Nr4a3*, which in humans are *NR4A1*, *NR4A2*, and *NR4A3*. They are widely expressed across various tissues and act as transcription factors regulating a wide range of cellular physiologies, including cell proliferation, apoptosis, and fuel utilization.[12] Interestingly, learning activities induce a fast increase in Nr4a1 (also known as NGFIB or Nur77) and Nr4a2 (also known as Nurr1 or Hzf-3) in the mouse hippocampal CA1 region,[13,14] and Nr4a2 in rat CA1 and CA3.[15] Transgenic mice expressing a dominant-negative Nr4a form (Nr4aDN) showed impaired contextual fear memory.[16] Repressing Nr4a1 and Nr4a2 expression by histone deacetylase-3 (HDAC3) activity also impaired cognitive functions, including object location and contextual memory,[14,16] suggesting that the expression of Nr4a proteins was correlated with cognition. In cognitively impaired aged rats, Nr4a1/2 could not be induced in the hippocampus by learning activities, indicating that the immediate early response of Nr4a1/2 was lost in those cognitively impaired animals.[14] These observations demonstrate that Nr4a proteins play a critical role in cognition. However, the underlying mechanisms by which Nr4a proteins regulate cognition remain unclear.

In the current study, we assessed the role of Nr4a1 in cognitive aging, focusing on excitatory synaptic functions. NR4A1 mRNA of peripheral blood mononuclear cells (PBMCs) declined with age in humans, especially in populations with cognitive defects. We also found that the NR4A1 mRNA level showed age-dependent reduction in the human hippocampus based on a published RNA-microarray dataset. Similarly, Nr4a1 was decreased in the PBMCs as well as in the brains of aged mice. The Nr4a1 level in the mouse hippocampal CA1 region exhibited a positive linear correlation with cognitive capacity. Both systemic and CA1 pyramidal neuron-specific knockout of Nr4a1 impaired the excitatory synaptic functions and the cognition of young mice, while Nr4a1 overexpression ameliorated the cognition of aged mice. We further demonstrated that Nr4a1 acted as a cognitive enhancer by pro-

RESEARCH IN CONTEXT

1. **Systematic review**: Orphan nuclear receptor subfamily 4 group A (NR4A in human and Nr4a in rodent) contains three immediate early genes, *Nr4a1*, *Nr4a2*, and *Nr4a3*. The brain expressions of rodent Nr4a increase quickly after learning activities. Expressing the dominant-negative Nr4a form (Nr4aDN) or repressing Nr4a by HDAC3 leads to impaired contextual fear memory in rodent, demonstrating the critical role of Nr4a in cognition. Blocking Nr4a impairs the later phase of long-term potentiation, which is considered as a cellular basis of learning and memory, indicating that Nr4a contributes to the gene expression period of synaptic plasticity. A recent study shows that the immediate expression increment of Nr4a1/2 after learning activity is deficient in aged mice with cognitive impairment, and transcriptomic study indicates that Nr4a1 is decreased in aged mouse brain. However, the pattern of reduction of Nr4a1 expression is unclear, and the cause of Nr4a1 reduction and cognitive decline with aging remains elusive.
2. **Interpretation**: NR4A1/Nr4a1 was reduced in the peripheral blood mononuclear cells in both aged humans and mice, and was severe in aged individuals with cognitive disorders. In addition, we demonstrated that Nr4a1, but not Nr4a2/3, was specifically decreased in the mouse hippocampal CA1 region and cortex. NR4A1 also declined with aging in the human hippocampus. We found that Nr4a1 ablation impaired the dendritic spine density and glutamate receptor expression in CA1, and led to synaptic dysfunction and cognitive injury. Overexpressing Nr4a1 in CA1 pyramidal neurons improved the cognition of aged mice. Intriguingly, Nr4a1/NR4A1 directly bound to TrkB promoter in both mouse and human genomic backgrounds, and induced the transcriptional activity of TrkB, which was necessary for Nr4a1-dependent cognitive enhancement.
3. **Future directions**: Our findings demonstrate the correlation between Nr4a1 and cognition, which suggests that human NR4A1 is a potential target for the early diagnosis and treatment of cognitive decline with age. The mechanisms of age-dependent NR4A1/Nr4a1 reduction will be investigated in future studies, and an NR4A1-based diagnosis and therapeutic strategy might become available for clinical use.

moting the transcription of tyrosine kinase receptor B (TrkB), which has been widely recognized to mediate neural differentiation, survival, neurogenesis, and long-term potentiation (LTP).[17,18] These results suggested that NR4A1 might serve as a biomarker for early diagnosis and an alternative therapeutic target in age-related cognitive impairment.

2 | METHODS

2.1 | Participants

A total of 40 subjects aged from 20 to 85 years were recruited from the Department of Neurology in the Affiliated Drum Tower Hospital of Nanjing University Medical School. Informed consent was obtained from all the participants and this study was approved by the ethics committee of Nanjing Drum Tower Hospital (2017-079-04). The participants were divided into the 20 to 40, 50 to 59, 60 to 69, and 70 to 85-year-old groups. Meanwhile, subjects over 50 years old were divided into a cognitive impairment group (n = 16) and a normal cognitive group (n = 14) according to the neuropsychological test results. All participants were right-handed. The exclusion criteria for all participants included illiteracy or refusing to complete the neuropsychological test; inability to give informed consent; any neurological disorders (stroke, AD, Parkinson's disease, family history of dementia, etc.); brain trauma; any psychiatric disorders or severe visual or hearing loss. All subjects underwent clinical information collection (gender, age, education, hypertension, etc.), a routine blood collection, and a comprehensive neuropsychological test using the Chinese version of the Mini-Mental State Examination (MMSE) and the Beijing version of Montreal Cognitive Assessment (MoCA) as a general cognitive function evaluation. The MMSE/MoCA scores both range from 0 to 30, and the lower scores represent worse cognitive status. Our cognitive impairment group was diagnosed when the MoCA score was ≤19 for persons with 1 to 6 years of education, ≤24 for those with 7 to 12 years of education, or ≤25 for persons with >12 years of education.[6,19]

2.2 | Animals and treatments

All animal procedures were approved by the Animal Care and Use Committee of the Model Animal Research Centre, Nanjing University. Male C57BL/6 mice were purchased from Nanjing Junke Bioengineering (China). *Nr4a1*-knockout (KO) mice (*Nr4a1*$^{-/-}$, strain name: *C57BL/6JGpt-Nr4a1*^{em52Cd2170}*/Gpt*) and mice carrying *Nr4a1*-floxed alleles (*Nr4a1*$^{fl/fl}$, strain name: *C57BL/6JGpt-Nr4a1*^{em1Cflox}*/Gpt*) were provided by GemPharmatech (China). *Nr4a1*$^{-/-}$ and *Nr4a1*$^{fl/fl}$ mice were on the C57BL/6 background. Age-matched wild type (WT) male littermates of *Nr4a1*$^{-/-}$ mice served as controls in *Nr4a1*$^{-/-}$ mouse-involving behavior or biochemical experiments. All experimental mice were fed a standard rodent diet at 20 to 25°C and kept on a 12-hour light and 12-hour dark cycle. All mice were housed at least 1 to 2 weeks before the behavioral testing. Stereotaxic injection of adult mice was performed as previously described.[20] Briefly, the mice were anaesthetized with 1.5% isoflurane in a 30% O_2/68.5% N_2O mixture and placed on a stereotaxic apparatus, and the skull was fully exposed. The needle was injected at −1.9 mm to the bregma on the anterior-posterior, ± 1.50 mm on the medial-lateral, and −1.53 mm on the dorsal-ventral axes. $AAV_{Nr4a1\text{-}EGFP}$, $AAV_{Cre\text{-}EGFP}$, and control AAV_{EGFP} (AAV stands for adeno-associated virus, EGFP for enhanced green fluorescent protein) were provided by OBiO Technology (China), and 200 nL AAV per injection was bilaterally injected into the CA1 region at a rate of 50 nL/min.

In the experiments with the administration of ANA12, a selective TrkB antagonist, 16 days after the stereotaxic injection of AAV, the mice were intraperitoneally injected with 0.5 mg/kg ANA12 (Selleck, China) in 200 μL saline each day for 14 days. The ANA12 was dissolved in dimethyl sulfoxide (DMSO). Mice of vehicle group were daily injected with an equal amount of DMSO in 200 μL saline at same time.

2.3 | Behavioral test

2.3.1 | Open field test

An open field test (OFT) was performed to evaluate autonomous, exploratory behavior and the mental tension of the mice in a novel environment. The mice were placed in a 40 cm × 40 cm × 15 cm box and allowed to freely explore for 10 min. The bottom of the box was divided into 4 × 4 grids. The total distance travelled and the time spent in the corner and central grids were recorded and further analyzed with ANY-maze software (Stoelting, USA).

2.3.2 | Contextual fear-conditioning test

To explore hippocampus-dependent memory, a contextual fear-conditioning (CFC) test was performed as previously described.[21] The mice were placed in a conditioning chamber (Panlab, Spain) for 5 minutes without any stimulation and subsequently twice received foot shocks (foot shock: 2 seconds, 0.75 mA, 1 minute between shocks). The mice were allowed to stay in the chamber for 1 minute after the shock to evaluate postshock freezing. Hippocampal-dependent memory was examined at 24 h after training. The mice were allowed to freely explore the same chamber for 5 minutes without any stimulation. The chamber was cleaned with 75% alcohol, and the freezing time was determined using Packwin software (Panlab).

2.3.3 | Morris water maze test

To examine spatial memory, the Morris water maze (MWM) test was performed as previously described.[22] The mice were placed in a circular water tank (120 cm in diameter, 40 cm in height) filled with water to a depth of 25 cm. A round platform (6 cm in diameter) was placed below the water surface. The mice were trained to find the platform within 1 minute (four trials per day) for 5 consecutive days. During

the training period, the platform was placed in the target quadrant. The escape latencies of four trials were averaged to determine a daily mean. On the sixth day, the platform was removed, and the mice were allowed to explore for 60 seconds in the two quadrants next to the target quadrant. The escape latency, the number of platform crossings and the time spent in the target quadrant were recorded with ANY-maze software (Stoelting). After each training or test, the mice were quickly dried with a towel and warmed under a heating lamp to avoid hypothermia.

2.3.4 | Y maze spontaneous alteration test

The Y maze spontaneous alteration (YM) test is widely used to evaluate short-term working memory. The YM consists of three identical arms installed in the shape of the letter "Y." Each arm was 40 cm in length and 8 cm in width, with walls that were 10 cm in height and made of opaque material. The mice were placed in the center of the YM and allowed to explore freely for 8 minutes. The order in which the mice passed into the arms during the exploration period was recorded. The correct ratio of alternative exploration of different arms in the YM was calculated.

2.4 | Blood collection and PBMC isolation

Blood samples were collected from humans and mice in ethylenediaminetetraacetic acid (EDTA) tubes, and PBMCs were isolated within 4 hours. The supernatant was removed after centrifugation at 1500 rpm for 10 minutes. The precipitate was resuspended in Dulbecco's modified Eagle's medium (DMEM; Gibco, USA) and gently added to the surface of 3 mL of lymphocyte-separating medium (TBD Science, China). The samples were centrifuged at 2000 rpm for 20 minutes and then gently collected and washed twice with DMEM to remove debris. Cells were resuspended in TRIzol reagent (Thermo Fisher Scientific, USA) and stored at −80°C for further analysis.

2.5 | Real-time quantitative polymerase chain reaction

Total RNA was extracted from PBMCs or fresh hippocampal CA1 brain tissue using TRIzol reagent (Thermo Fisher Scientific) and reverse-transcribed into cDNA using HiScript III RT SuperMix (Vazyme, China) according to the manufacturer's instructions. Real-time quantitative polymerase chain reaction (RT-qPCR) was performed on a Roche Light Cycler 96 (Roche, Switzerland) with SYBR Green (Applied Biosystems, USA). Relative gene expression was analyzed by the $2^{-(\Delta\Delta Ct)}$ method, and the levels were normalized to that of GAPDH. The primers used are listed in Table S1.

2.6 | Immunofluorescence staining

The mice were sacrificed under deep anesthesia and perfused with cold saline, followed by 4% formaldehyde. After being soaked in 15% and 25% sucrose (in 0.1 M phosphate-buffered saline [PBS]) successively, the brains were frozen and sliced into 20 μm sections using a rotary microtome (Leica, Germany). Frozen brain slices were permeabilized with 0.25% Triton X-100 (in 0.1 M PBS), blocked with 2% bovine serum albumin (BSA; in 0.1 M PBS) and then incubated with anti-Nr4a1 (sc-166166, Santa Cruz Biotechnology, USA) and anti-NeuN (ab177487, Abcam, USA) primary antibodies overnight at 4°C. After being washed three times, the slices were incubated with secondary antibodies (Invitrogen, USA) for 2 hours at room temperature. DAPI (1 mg/mL) (Bioworld, USA) was used to stain cell nuclei. A confocal microscope (FV3000, Olympus, Japan) was used to obtain fluorescence images. The images were further analyzed by ImageJ v1.8 software (National Institutes of Health, USA).

2.7 | Western blotting

Tissue lysate was prepared and subjected to western blotting as previously described.[23] Equal amounts of protein were subjected to SDS-PAGE and transferred to polyvinylidene difluoride (PVDF) membranes (Millipore, USA). After being blocked in 5% skim milk for 1.5 hours at room temperature, the membranes were incubated overnight at 4°C with primary antibodies (the information for antibodies is in Table S2). The membranes were subsequently incubated with the corresponding secondary antibodies (Bioworld) and visualized with western blotting chemiluminescent substrate (WBKLS0500, Millipore).

2.8 | RNAscope in situ hybridization

Mouse brains were cut into 15 μm slices on Superfrost Plus microscope slides (Thermo Fisher Scientific). In situ hybridization (ISH) was performed according to the RNAscope 2.5 HD Assay-Red Detection Kit (Advanced Cell Diagnosis, USA). Briefly, hydrogen peroxide was added to the slices for 10 minutes at room temperature, and the slices were incubated with target retrieval reagents (322350, Advanced Cell Diagnosis) for 5 minutes at 100°C. A hydrophobic pen was used to create a barrier around each brain section. The sections were incubated with Protease Plus solution for 30 minutes at 40°C using the HybEZ Hybridization System (Advanced Cell Diagnostics) and then washed in distilled water. The slices were incubated with RNAscope Probe-Mm-Nr4a1 (Advanced Cell Diagnosis) for 2 hous at 40°C, incubated with a series of six amplifier probes (30 minutes each for steps 1 and 3, 15 minutes each for steps 2 and 4 at 40°C, 30 minutes for step 5, and 15 minutes for step 6 at room temperature), and washed with the wash buffer provided with the kit between each step. Finally, the sections were incubated with RED working buffer (RED-B: RED-A = 1:60) for

10 minutes at room temperature and then mounted with Vector Labs VectaMount (Advanced Cell Diagnostics) for further analysis.

2.9 | Electrophysiology

2.9.1 | Single-cell genetic manipulation for patch-clamp recording of hippocampal slices

To achieve single-cell deletion or overexpression of Nr4a1 in CA1 pyramidal neurons (PyrNs), we used $AAV_{Cre\text{-}mCherry}$ or $AAV_{Nr4a1\text{-}EGFP}$, $LV_{TrkB\text{-}EGFP}$ (OBiO Technology; LV stands for lentivirus), which specifically expressed target genes with porcine teschovirus-1 2A (P2A)-separated fluorescent tags in excitatory neurons, respectively, with $Nr4a1^{fl/fl}$ or Nr4a1-KO mice as the background. The procedures were performed as described in a previous study.[24] Briefly, the mice were stereotactically injected with high-titer AAV (more than 10^{13} IU/mL) or LV (more than 10^{8} IU/mL) into the CA1 region on postnatal day 0 (P0). P0 mice were anaesthetized via immersion in ice for 5 minutes and then fixed in a custom plasticine mold to adjust the bregma and lambda to be horizontal. Lambda was regarded as the zero points of the X and Y axes (X axis leftward and Y axis anterior were positive values). The zero point of the Z axis was the position at which the needle penetrated the skin. There were seven sites for injection in each hemisphere, including (X, Y) = (± 1.2 mm, 1.2 mm) and Z downward at 1.4 mm, 1.0 mm, and 0.6 mm, and (X, Y) = (± 1.5 mm, 1.0 mm) and Z downward at 1.7 mm, 1.3 mm, 0.9 mm, and 0.5 mm. Approximately 10 nL of AAV or LV solution was injected into each site with a beveled glass injection pipette connected to a microsyringe (BR,I-235, Sutter Instrument Co., USA). The injected mice were placed back in their cages and used for recordings on P19~28.

2.9.2 | Preparation of acute hippocampal slices

The field excitatory postsynaptic potential (fEPSP) LTP of Nr4a1-KO mice (P19~28) and the various electrophysiological parameters of single-cell Nr4a1 deletion or Nr4a1 or TrkB overexpression in CA1 PyrNs were recorded in acute hippocampal slices. Hippocampi were sectioned into 350-μm slices with a vibratome (VT1000 S, Leica) in high-sucrose cutting solution containing 2.5 mM KCl, 1.25 mM NaH_2PO_4, 25 mM $NaHCO_3$, 0.5 mM $CaCl_2$, 7 mM $MgSO_4$, 210 mM sucrose, 10 mM D-glucose, and 1.3 mM Na-ascorbate (all from Sigma-Aldrich, USA). Fresh slices were placed in an incubation chamber and were soaked in artificial cerebrospinal fluid (ACSF; 119 mM NaCl, 2.5 mM KCl, 2.5 mM $CaCl_2$, 1.3 mM $MgSO_4$, 26.2 mM $NaHCO_3$, 1 mM NaH_2PO_4, and 11 mM D-glucose), maintained at 32°C for 20 minutes and placed at room temperature for 60 minutes for recovery before recording. All cutting solutions and ACSF that were used for slice preparation and patch-clamp recording were saturated with oxygen and maintained at pH 7.3 to 7.4 through consistent buffering with 95% O_2/5% CO_2.

2.9.3 | Recording of fEPSP LTP

Well-prepared acute hippocampal slices were placed in the recording chamber and perfused with ACSF containing the GABAA receptor antagonists picrotoxin (PTX, 100 μM, Tocris, UK) and bicuculline (Bic, 10 μM, Absin, China). The recording electrode, which was filled with ACSF and had 1 to 2 MΩ resistance, and a concentric bipolar stimulation electrode (CBBRC75, FHC, USA) were placed at the stratum radiatum and ≈200 μm apart. The fEPSPs of SC-CA1 synapses were evoked by current injection through the stimulation electrode. The baseline was set as 40% of the maximum fEPSP. At least 20 minutes of steady baseline was recorded, and then high-frequency stimulation (HFS; 3 trials of 100 Hz/s pulses with 20-second intervals) was used to induce LTP. After HFS, 60-minute fEPSPs evoked by the same stimulating density as baseline were recorded. The fEPSP recording frequency was 4 trials/min. The rise slope of the fEPSP was obtained and used for statistical analysis.

2.9.4 | Whole-cell dual-electrode recording in acute hippocampal slices

For all evoked postsynaptic current recordings, a concentric bipolar stimulation electrode was placed at the stratum radiatum, where the SC is located. Recording electrodes (3 to 6 MΩ) were filled with the internal solution containing 135 mM $CsMeSO_3$, 8 mM NaCl, 10 mM HEPES, 0.3 mM EGTA, 4 mM Mg-ATP, 0.3 mM Na_3-GTP, 5 mM QX-314, and 0.1 mM spermine, and simultaneously patched to AAV-infected PyrNs with a fluorescent tag and a neighboring uninfected control (Ctrl) PyrN at the CA1 stratum pyramidale. For AMPA receptor (AMPAR)- and NMDA receptor (NMDAR)-evoked excitatory postsynaptic currents (eEPSCs) and paired-pulse ratio (PPR) recordings, hippocampal slices were perfused with ACSF supplemented with 100 μM PTX and 10 μM Bic, and the stimulation was set as the intensity that evoked measurable, monosynaptic EPSCs. AMPAR-eEPSCs were obtained as the peak amplitude at −70 mV holding. NMDAR-eEPSCs were obtained as the amplitude at 150 ms after stimulation with +40 mV holding. The PPR was the ratio of two peak amplitudes with a 50 ms interval (peak 2/peak 1) at −70 mV holding. To obtain the rectification index (RI) of AMPAR, the GABAA receptor antagonists and the NMDAR antagonist D-AP5 (100 μM, Alomone, Israel) were added to the ACSF. With this condition, eEPSC peak amplitudes were recorded at −70 mV (I_{-70}), 0 mV (I_0) and +40 mV (I_{+40}) holding, and $RI = [(I_{+40} - I_0)/40]/[(I_{-70} - I_0)/-70]$. Miniature EPSCs (mEPSCs) were recorded in whole-cell gap-free mode at −70 mV holding using the same internal solution as that for the eEPSC recording. While recording mEPSCs, 100 μM PTX, 10 μM Bic, 100 μM D-AP5, and 1 μM tetrodotoxin (TTX, Absin) were all added to ACSF to assess the pure AMPAR-mediated, synapse-driven spontaneous response. To record evoked inhibitory postsynaptic currents (eIPSCs), the ACSF was supplemented with 100 μM D-AP5 and 10 μM NBQX (AMPAR antagonist, Alomone). The eIPSCs were obtained as the peak amplitude at 0 mV holding.

The whole-cell recording of LTP was based on AMPAR-eEPSC recordings. Three- to five-minutes steady baseline AMPAR-eEPSCs were recorded, and then LTP was induced by 2 Hz/90 seconds pairing stimulation while holding at 0 mV, which was performed within 6 minutes after breaking into the cell.[25,26] After pairing, 60-minute AMPAR-eEPSCs were recorded. The eEPSC recording frequency was 4 trials/min. It was worth mentioning that to minimize the run-up during baseline recording, the patched cells were held in a cell-attached state for 1 to 2 minutes before being broken into.

2.9.5 | Primary hippocampal neurons and cell lines

P0 C57BL/6JGpt mice (provided by GemPharmatech) were sacrificed to obtain the hippocampi. The separated hippocampi were then digested with 0.25% trypsin and resuspended in DMEM/F12 medium (Gibco) containing 10% fetal bovine serum (FBS, Gibco). Cells were plated at a density of 10^6 cells/mL on poly-D-lysine-precoated glass slides (Thermo Fisher Scientific). Within the first 4 hours of plating, the cells were cultured in 10% FBS-DMEM/F12 medium, and then placed in Neurobasal-based medium with 2% B27, 1% GlutaMAX, 37.5 mM NaCl, 0.3% W/V D-glucose, and penicillin/streptomycin (commercial cell-culture mediums and reagents are all from Gibco) for the rest of the culture period; half of the medium was exchanged every 2 days. The plasmid vector of CRISPR/Cas9 targeting the Nr4a1-binding site of the TrkB promoter and the backbone Cas9 vector without the sgRNA array were transfected into primary cultured neurons with Lipofectamine 2000 transfection reagent (Invitrogen) 3 days after cell plating.

N2a, SH-SY5Y neuroblastoma cells and HEK293T cells were purchased from Zhong Qiao Xin Zhou Biotechnology (China) and cultured in DMEM (Gibco) containing 10% FBS and 1% penicillin/streptomycin.

2.9.6 | Construction of CRISPR/Cas9 targeting the Nr4a1-binding site of the TrkB promoter

We used the CCTop-CRISPR/Cas9 target online predictor[27] to list all possible single guide (sg)RNAs to target the −2114 to −1794 bp fragment of the TrkB promoter. Three sgRNA target sites that were evenly distributed along the binding site were selected, including sg1: 5′-GGTGAGAGGAGGCTCAGATC-3′ (−2105 to −2086 bp 5′ upstream of ATG); sg2: 5′-GCTGGAAGCACATCCTGCCT-3′ (−1960 to −1941 bp 5′ upstream of ATG); and sg3: 5′-GCTGGAAGCACATCCTGCCT-3′ (−1840 to −1821 bp 5′ upstream of ATG). Three sgRNAs and the respective U6 promoter and sgRNA scaffold were arranged in order and inserted into the Cas9-coding backbone vector *pFugw-Ubi-mCherry-P2A-Cas9*.

The CRISPR/Cas9 vectors described above were delivered into N2a cells, which had plated in 3.5 cm 0.1 mg/mL poly-D-lysine-precoated dishes and been at ≈70% confluence, with Lipofectamine 2000. We obtained N2a genomic DNA 72 hours after transfection through phenol chloroform. The targeted region was amplified by a pair of primers flanking the predicted Nr4a1-TrkB promoter binding site. The primers were CRISPRseq-F, 5′-CGTGCTGGGTTTCTTCTC-3′ and CRISPRseq-R, 5′-CATGCTCATAGGGGAAAG-3′. We then cloned the PCR products into pMD19-T vector (TAKARA, Japan) and sequenced the inserted fragments via the Sanger method (carried out by Genwiz, China).

2.9.7 | Recording the mEPSCs of primary cultured hippocampal neurons

Cultured neurons were used for patch-clamp recording on days 14 to 21 after plating. The neuron slides were placed in the extracellular solution containing 145 mM NaCl, 5 mM KCl, 1 mM $CaCl_2$, 1 mM $MgCl_2$, 5 mM D-glucose, 25 mM sucrose, 5 mM HEPES, 0.1 mM PTX, 0.1 mM D-AP5, and 0.001 mM TTX, and adjusted to pH 7.3 with NaOH. The slides were then patched with a 3 to 6 MΩ recording electrode filled with an internal solution containing 140 mM CsCl, 2 mM $MgCl_2$, 10 mM HEPES, 5 mM EGTA, 0.3 mM Na_3-GTP, and 4 mM Na_2-ATP, and adjusted to pH 7.3 with KOH. When recording mEPSCs, extracellular solution supplemented with 200 mM sucrose was buffered towards the patched neurons to induce more mEPSCs. Two minutes of mEPSCs were recorded in whole-cell gap-free mode at −70 mV holding.

In all patch-clamp electrophysiological experiments, the data were recorded with a Multiclamp 700B amplifier and Digidata 1550 data acquisition system (Axon Instruments, USA), filtered at 2 kHz, and digitized at 50 kHz.

2.10 | Golgi staining

Golgi staining was performed as previously described[28] with an FD Rapid Golgi staining kit (FDNeuroTechnologies, Columbia, USA) according to the manufacturer's instructions. The kit consisted of solutions A to E. The brain was rapidly immersed in a mixture of solutions A and B and stored for 2 weeks (changed once within 24 hours) at room temperature in the dark to avoid decomposition. Then, the samples were transferred into solution C for at least 3 days. The brain was then cut into 100-μm thick sections using a cryostat microtome (Leica). The sections were further stained according to the kit instructions. Images were observed and captured by an inverted microscope (IX73, Olympus) and analyzed by ImageJ v1.8 software.

2.11 | Cleavage under targets and tagmentation assay

The cleavage under targets and tagmentation (CUT&Tag) assay was performed as described previously with some modifications.[29] Hippocampal CA1 tissue samples were collected from 3-month-old WT mice. Briefly, 10 μL of concanavalin A-coated magnetic beads (Bangs Laboratories, USA) were added to each sample and incubated at room temperature for 10 minutes. Bead-bound cells were resuspended in a 1:50 dilution of anti-Nr4A1 (sc-166166, Santa Cruz Biotechnology) antibodies or IgG Ctrl antibodies (normal mouse IgG, 12-371, Mil-

lipore) and incubated on a rotating platform overnight at 4°C. The primary antibodies were removed, and the sample was incubated with secondary antibodies (rabbit antimouse IgG H&L, ab611709, Abcam) at room temperature for 60 minutes. The secondary antibodies were removed, and the sample was incubated with a pA-Tn5 adapter complex at room temperature for 1 hour. The sample was washed and resuspended in tagmentation buffer and incubated at 37°C for 1 hour. DNA was purified using phenol-chloroform-isoamyl alcohol extraction and ethanol precipitation. Sequencing was performed in an Illumina (USA) NovaSeq 6000 using 150 bp paired-end sequencing according to the manufacturer's instructions. The BAM file was generated by the unique mapped reads as an input file using Macs2 software for call-peak with a cutoff value of <0.05. HOMER's find Motifs Genome.pl tool was used for motif analysis. The input file was the peak file and the genome FASTA file. The DNA sequence was extracted according to the peak file, and the sequence was compared with the Motif database to obtain the Motif. Read distributions (from BigWig) across genes are presented as a heatmap. Genes were represented as lines that were sorted in descending order based on signal intensity. The deepTools tool was used for this analysis (Shanghai Jiayin Biotechnology, China). The systemic information of Nr4a1-binding peak-adjacent Gene Ontology (GO) and Kyoto Encyclopedia of Genes and Genomes (KEGG)-pathway enrichment and motif results are presented as separate supplementary files named *CUT&Tag Material 1. Peak-adjacent GO and pathway enrichment* and *CUT&Tag Material 2. Motif results*, respectively. *CUT&Tag Material 1. Peak-adjacent GO and pathway enrichment* is an Excel file containing the systemic information of biological progress (Sheet 1–2), cellular component (Sheet 3–4) and molecular function (Sheet 5–6) GO enrichment analyses, and KEGG-pathway enrichment analysis (Sheet 7–8). *CUT&Tag Material 2. Motif results* is a Word file containing Known (CUT&Tag Table 1) and *de novo* (CUT&Tag Table 2) motif details at Nr4a1-binding peak regions.

2.12 | Chromatin immunoprecipitation

Chromatin immunoprecipitation (ChIP) was performed according to the instructions of the SimpleChIP Enzymatic Chromatin IP Kit (9003, Cell Signaling Technology, USA) with some modifications. Briefly, fresh hippocampal CA1 tissues (25 mg) or SH-SY5Y cells were collected and cross-linked in 1% formaldehyde. The sample was then broken down into a single-cell suspension by a Dounce homogenizer for further nuclear preparation and chromatin digestion to 150 to 9900 bp using micrococcal nuclease. Then, the lysate was sonicated with three pulses for 10 seconds and incubated with 1.5 μg of antimouse Nr4a1 (sc-166166, Santa Cruz Biotechnology) antibodies or control mouse IgG (CS200621, Millipore) for mouse CA1 samples, or antihuman NR4A1 (NB100-56745, Novus, USA) or control human IgG (2729s, Cell Signaling Technology) for SH-SY5Y samples, overnight at 4°C. The antibodies were immobilized on 30 μL of ChIP-Grade Protein G Magnetic Beads for 2 hours. DNA was eluted from antibody/Protein G Magnetic Beads, and the crosslinks were reversed and purified using spin columns for qPCR. The ChIP primers are presented in Table S2 in the Supporting Information file.

2.13 | Dual-luciferase reporter assay

HEK293T cells were incubated with the Nr4a1 (mouse)/NR4A1 (human)-overexpressing plasmid or empty vectors (GeneChem, China) for 24 hours, while N2a cells were incubated with the Nr4a1-knockdown shRNA plasmid and control vectors (GeneChem). The *Ntrk2* (mouse)/*NTRK2* (human) promoter and Nr4a1-binding region of the truncated Ntrk2 promoter were cloned into the pGL3-promoter vector with a luciferase reporter gene (Promega, USA). The luciferase reporter plasmid (1.0 μg) and TK-Renilla (0.1 μg) were cotransfected into HEK293T cells or N2a cells in 24-well plates using Lipofectamine 3000 (L3000015, Invitrogen). After 18 hours of incubation, firefly/Renilla luciferase activities were measured by a dual-luciferase reporter system (E2920, Promega).

2.14 | Statistical analysis

The data were presented as the mean ± SEM and analyzed using GraphPad Prism 9 (GraphPad, USA). Statistical differences were determined by one-way analysis of variance (ANOVA) followed by post hoc multiple-comparisons tests (Tukey's correction) to analyze differences among three or more groups with one independent variable, by two-way ANOVA followed by post hoc multiple-comparisons tests (Tukey's correction) to analyze differences among three or more groups with two independent variables, or by unpaired Student *t*-test to analyze differences between two groups, apart from dual-electrode patch-clamp recording with a paired *t*-test. $P < 0.05$ was considered statistically significant.

3 | RESULTS

3.1 | Age-dependent NR4A1/Nr4a1 reduction in PBMCs in humans and mice

To investigate the relationship between NR4A1 and aging, we examined the NR4A1 mRNA level by RT-qPCR in PBMCs from individuals aged 24 to 83 years. The results showed that the level of NR4A1 decreased with aging (Figure 1A). Intriguingly, among individuals over 50 years old, the mRNA level was significantly lower in individuals with cognitive disorders than that in individuals with normal cognition (Figure 1B), although there was no significant difference between the ages (Figure 1C). Notably, NR4A2 and NR4A3, the other molecules of the NR4A family, were stably expressed in the PBMCs of individuals at different ages (Figure 1D,E). These results suggest that Nr4a1 expression in peripheral blood is decreased with age, which is exacerbated in people featuring cognitive disorders.

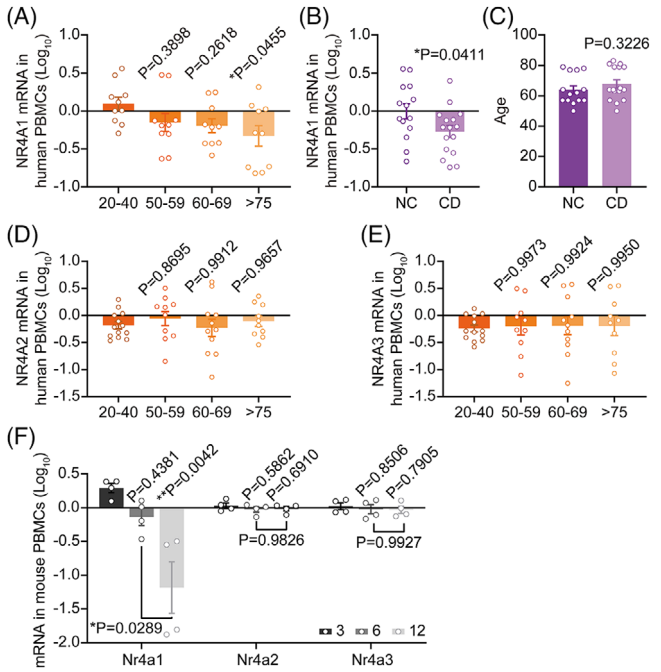

FIGURE 1 Aging-related and cognition-associated NR4A1 reductions in human and mouse peripheral blood mononuclear cells (PBMCs). (A) Bar graph showing the logarithmic comparison of NR4A1 mRNA in PBMCs from humans of different ages. Dots indicate the $\log_{10}$(individual/average of all individuals), and columns with error bars present the mean ± SEM. $n = 10$ per group. Each group assessed vs 20 to 40-year-olds; one-way ANOVA. (B) Logarithmic comparison of NR4A1 mRNA in PBMCs from >50-year-old individuals divided into normal cognition (NC) and cognitive disorder (CD) groups. $n = 14$ in the NC group, $n = 16$ in the CD group. Two-tailed unpaired *t*-test. (C) Ages of NC and CD groups. Two-tailed unpaired *t*-test. (D,E) Bar graphs showing the logarithmic comparison of NR4A2 and NR4A3 mRNA in the PBMCs from human individuals at different ages. $n = 10$ to 12. The *P*-values indicate comparisons to the 20 to 40 age group, one-way ANOVA. (F) Bar graph showing the logarithmic comparison of Nr4a1, Nr4a2, and Nr4a3 mRNA in PBMCs of 3-, 6-, and 12-month-old mice. $n = 4$ per column, one-way ANOVA. The *P*-values above the columns were from the comparison to 3-month-olds, and the *P*-values below the columns indicate 6- vs 12-month-old mice.

Nr4a1 in mouse PBMCs was significantly decreased in 12-month-old mice compared with 3- and 6-month-old mice, while Nr4a2 and Nr4a3 showed no statistical difference among these age groups (Figure 1F). These results indicate that Nr4a1 is expressed with an age-related pattern in both human and mouse PBMCs.

3.2 | Age-dependent Nr4a1 decline in the brain

We examined the relationship between aging and cognition in mice. As expected, 12-month-old mice displayed impairments in both contextual memory and short-term working memory, as detected by the CFC and YM tests, respectively, compared to 3-month-old mice (Figure S1A,D,I). We also observed a modest reduction in the CFC freezing rate in 6-month-old mice (Figure S1I). No statistically significant differences were found in the parameters of the MWM (Figure S1E–H), indicating that the spatial learning ability had not been impaired at 12 months of age. It should be noted that mice at ages of 3 to 12 months showed no difference in locomotion and time spent in the center region in the OFT (Figure S1B,C), suggesting that the defects in cognition-related tests were caused by cognitive impairment but not mobility or psychiatric conditions.

Next, we examined the expression pattern of Nr4a1 in the mouse brain using immunofluorescence tests and ISH. Nr4a1 was widely expressed in the brains of 3-month-old mice (Figure 2A). In the hippocampus, the Nr4a1 protein level was higher in the neurons in CA1 stratum pyramidale than in the neurons in CA3 and dentate gyrus (DG) (Figure 2B). In addition, Nr4a1 was primarily located in the CaMKII-positive PyrNs in CA1 (Figure S2). Nr4a1 in CA1 was significantly decreased in 12-month-old mice compared to 3-month-old animals (Figure 2B,C,G–I, and Figure S3A,B). In contrast, Nr4a1 in the CA3 region and DG was not affected by aging (Figure 2B,C and Figure S3A,C,D). In addition, Nr4a1 was highly expressed in the cortex and exhibited an age-dependent decrease (Figure 2B,C and Figure S3A,E). Logarithmic values of the freezing rate of the CFC, but not the latency of the MWM, were linearly correlated with Nr4a1 fluorescence intensity in CA1 (Figure 2D,F). However, the correct rate of YM tests, which was significantly lowered in 12-month-old mice (Figure S1D), showed no statistically significant linear correlation with the Nr4a1 level (Figure 2E). Thus, the correlation analysis suggested a correlation between Nr4a1 expression in CA1 and cognition, particularly contextual memory. To exclude the effect of sex hormone-mediated differences in cognition and expression pattern with aging,[30,31] we used male mice for most of our experiments. Actually, we observed Nr4a1 decline in the CA1 of female mice (Figure S4), indicating that the alteration of Nr4a1 with aging was probably not gender dependent. We examined the levels of Nr4a2 and Nr4a3 via RT-qPCR and immunofluorescent tests, and found that their expressions were unaltered by aging not only in the mouse hippocampal CA1 but also in the CA3, DG, and cortex (Figure 2I–M), implying a specific role of Nr4a1 in age-related memory decline of mice.

Furthermore, we evaluated the NR4A1/2/3 expression patterns in three cognition-related brain regions, the hippocampus, amygdala, and medial prefrontal cortex (mPFC) of human, based on a published Gene Expression Omnibus (GEO) dataset, GSE25219.[32] NR4A1 expression exhibited a negative linear relation with age in human hippocampal samples from individuals of 18 to 70 years old (Figure S5A). Intriguingly, NR4A2 expression in the human hippocampus was negatively related to age, which was inconsistent with the mice data (Figure S5A). NR4A3 expression was steady with aging in the human hippocampus (Figure S5A). However, we did not observe any statistical differences in the expression of NR4A1, NR4A2, and NR4A3 with aging in human amygdala and mPFC samples (Figure S5B,C). These results indicate that the age-dependent NR4A1 decline in the hippocampus is a common pathological feature in the brains of humans and mice.

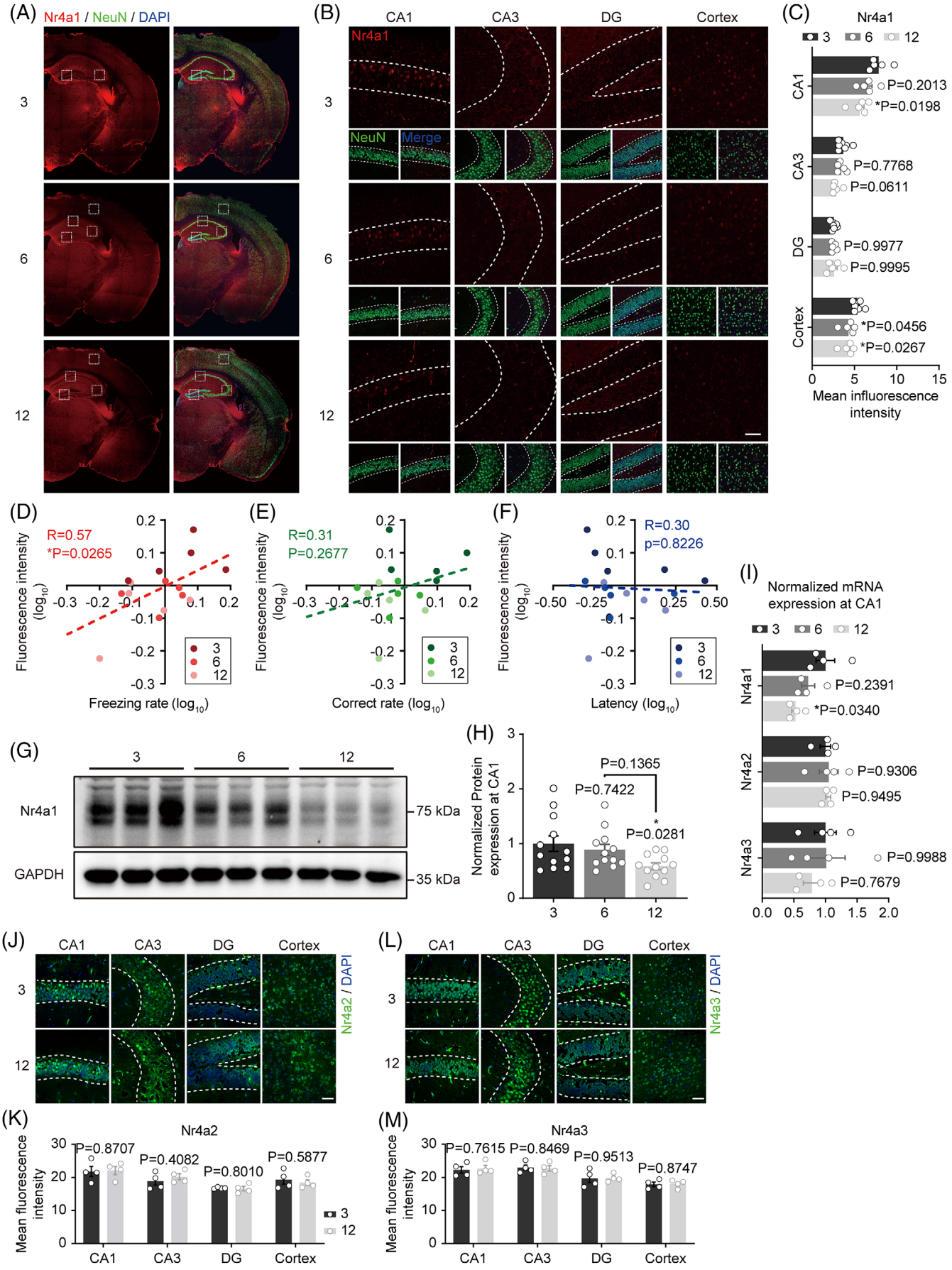
(A)
Nr4a1 / NeuN / DAPI
3
6
12
(B)
CA1
CA3
DG
Cortex
Nr4a1
NeuN
Merge
(C)
Nr4a1
3 6 12
CA1
P=0.2013
*P=0.0198
CA3
P=0.7768
P=0.0611
DG
P=0.9977
P=0.9995
Cortex
*P=0.0456
*P=0.0267
Mean influorescence intensity
(D)
R=0.57
*P=0.0265
Fluorescence intensity (log10)
Freezing rate (log10)
(E)
R=0.31
P=0.2677
Correct rate (log10)
(F)
R=0.30
p=0.8226
Latency (log10)
(G)
Nr4a1
GAPDH
75 kDa
35 kDa
(H)
Normalized Protein expression at CA1
P=0.1365
P=0.7422
*P=0.0281
(I)
Normalized mRNA expression at CA1
Nr4a1
P=0.2391
*P=0.0340
Nr4a2
P=0.9306
P=0.9495
Nr4a3
P=0.9988
P=0.7679
(J)
Nr4a2 / DAPI
(L)
Nr4a3 / DAPI
(K)
Nr4a2
Mean fluorescence intensity
P=0.8707
P=0.4082
P=0.8010
P=0.5877
(M)
Nr4a3
P=0.7615
P=0.8469
P=0.9513
P=0.8747

3.3 | Nr4a1 in hippocampal CA1 regulates cognition

To test whether Nr4a1 was required for cognitive maintenance, we generated Nr4a1-KO mice (Figure 3A). Behavioral analysis of 3-month-old Nr4a1-KO mice showed deficiencies in both contextual memory-associated CFC tests (Figure 3B) and working memory-associated YM tests (Figure 3C). The spatial memory-associated MWM test was not affected (Figure 3D–G), indicating that spatial memory might be more tolerated to Nr4a1 deletion. LTP is widely recognized as the physiological basis of learning and memory. The LTP of SC-CA1 synapses in Nr4a1-KO mice was significantly weaker than that in WT mice (Figure 3H,I). These results demonstrate that systemically deleting Nr4a1 induces cognitive impairment even in young mice.

To address whether deleting Nr4a1 in CA1 neurons caused cognitive impairment, we constructed a CA1 PryN-specific Nr4a1 knockout model (Nr4a1-cKO) through stereotactic injection of Cre-carrying AAV ($AAV_{Cre\text{-}EGFP}$, Cre and EGFP driven by the CamKII promoter) into the CA1 region of $Nr4a1^{fl/fl}$ mice (Figure 4A,B). The level of Nr4a1 was significantly decreased in the CA1 regions of Nr4a1-cKO mice (Figure 4C,D). Nr4a1-cKO mice showed deficits in both the CFC (Figure 4E) and YM tests (Figure 4F) but not in the MWM test (Figure 4G–J), which was consistent with the results from Nr4a1-KO mice. These results demonstrate that Nr4a1 in CA1 PyrNs is important to cognition.

Next, we tested whether Nr4a1 overexpression in CA1 PyrNs could ameliorate age-associated memory declines in old mice. AAV carrying Nr4a1 under CamKII promoter ($AAV_{Nr4a1\text{-}EGFP}$) was constructed and injected into the hippocampal CA1 region in WT mice at the age of 12 months (Figure 4K–M), and the cognition was evaluated by CFC and YM tests. Nr4a1 overexpression ameliorated both contextual fear memory and working memory decline in the CFC and YM tests (Figure 4N–Q). These results suggest that Nr4a1 overexpression in CA1 neurons enhances learning and memory functions in old mice. Taken together, these results demonstrate that Nr4a1 in CA1 PyrNs positively regulates cognitive functions.

3.4 | Nr4a1 ablation impairs synaptic conformation

We then analyzed the morphology of PyrNs to investigate the neuronal basis for Nr4a1-associated cognitive regulation. Golgi staining showed that Nr4a1 KO reduced the mature mushroom-type spines but not thin and stubby spines of CA1 PyrNs (Figure 5A,B). The total spine density was not significantly changed in CA1 PyrNs (Figure 5B). The spine densities of PyrNs in other regions, including the CA3 region, DG, or cortex, were not different between WT and KO mice (Figure 5C–E). Several synaptic proteins in hippocampal CA1 tissue were analyzed via western blotting. Nr4a1 KO reduced the glutamate receptor subunits GluA1, GluA2, GluN2A and GluN2B but not GluN1 (Figure 5F,G). The postsynaptic scaffold protein postsynaptic density 95 (PSD95) was also decreased (Figure 5F,G). Nevertheless, neither synaptic plasticity-related CamKII α/β nor presynaptic synaptophysin (SYP) were significantly decreased (Figure 5F,G). These data indicate that Nr4a1 KO decreases the level of glutamate receptors and the density of mature-form synapses in the CA1 region, which may lead to the impairment of synaptic conformation.

3.5 | Nr4a1 deficiency impairs excitatory synaptic transmission and plasticity

Synaptic transmission, plasticity, and intrinsic excitability are the bases of neuronal function. We achieved single-neuron deletion of Nr4a1 via stereotactic injection of AAV-mediated Cre recombinase ($AAV_{Cre\text{-}mCherry}$) into the hippocampal CA1 region of $Nr4a1^{fl/fl}$ mice on P0 (the day of birth). Cre-mCherry was driven by the CamKII promoter to ensure its expression in excitatory PyrNs. Acute hippocampal slices were prepared from P19 to 28 mice, and dual whole-cell recordings were made from pairs of infected Cre-mCherry-expressing neurons (Cre) and neighboring uninfected control (Ctrl) neurons simultaneously (Figure 6A). AMPAR-eEPSCs were significantly reduced in Nr4a1-deficient neurons (Figure 6B,C). In addition, Nr4a1 deletion did not alter the RI (Figure 6D), indicating that the Ca^{2+}-impermeable GluA2-containing assembly of AMPAR was not changed.[33] The mEPSC amplitude was decreased in Nr4a1-deficient neurons (Figure 6E), but the frequency remained unchanged (Figure 6F), which suggested that the attenuation of excitatory synaptic transmission was mainly caused by a reduction of AMPAR in the postsynaptic area. Nr4a1 ablation also reduced NMDAR-eEPSCs (Figure 6G,H). The PPR of AMPAR-eEPSCs was not changed (Figure 6K), suggesting that postsynaptic deletion of Nr4a1 did not affect presynaptic excitatory neurotransmitter release. In addition, Nr4a1-deleted neurons showed no changes in eIPSCs (Figure 6I,J). We also examined the action potentials (APs) with −0 to 200 pA step-current injection stimulations. Under the same stimulation intensity, Cre-expressing neurons and neighboring uninfected Ctrl neurons showed no differences in evoked-spike quantities (Figure 6L). In addition, the rheobase of current stimuli to evoke APs (Figure 6M)

FIGURE 2 Hippocampal CA1-enriched Nr4a1 declined with aging and correlated linearly with cognition. (A) Nr4a1 localization in the hemispheres of 3-, 6-, and 12-month-old mice. (B) Enlarged views of dashed regions in the left images of panel A. Scale bar = 50 μm. (C) Nr4a1 immunofluorescence intensity in the subregions. $n = 5$ to 7 for each age group. *P*-values next to the bars present the relevant comparisons with the 3-month-old group. (D–F) Linear correlations of the $\log_{10}$(individual/average of all individuals) of behavioral parameters and the Nr4a1 immunofluorescence intensity in the CA1. $n = 5$ per age group. (G,H) Protein level of Nr4a1 in the CA1 determined by Western blotting. $n = 12$ per group. (I) Nr4a1, Nr4a2, and Nr4a3 mRNA expression in the CA1 measured by RT-qPCR. $n = 4$ per group. (J–M) Nr4a2 and Nr4a3 immunofluorescence intensity in different brain regions. 3- vs 12-month-old samples of the same brain regions. $n = 4$ for each age group. In bar graphs of this figure, dots indicate individual values, and columns with error bars present the mean ± SEM. Panels C, H, and I are based on one-way ANOVA, and panels K and M on two-tailed unpaired *t*-tests.

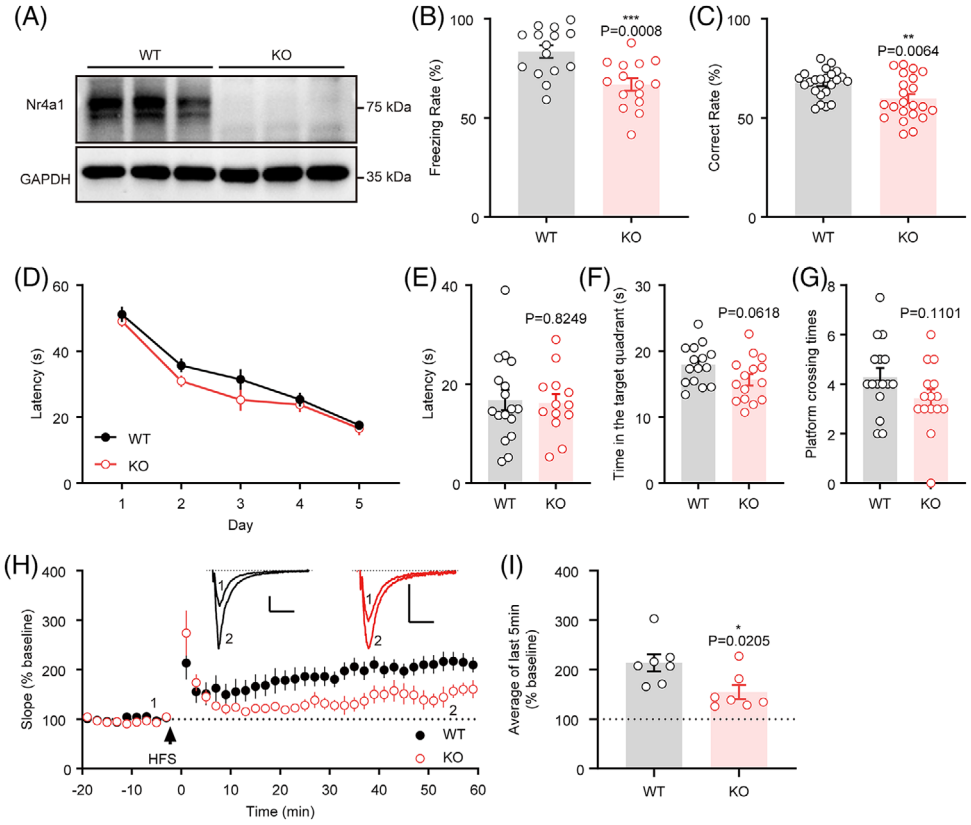

FIGURE 3 Systemic deletion of Nr4a1 diminished contextual and working memory and reduced the range of long-term potentiation (LTP). (A) The protein levels of Nr4a1 in the CA1 regions of wild type (WT) and systemic Nr4a1-knockout (KO) mice were determined by western blotting. (B) Bar graph showing the freezing rate in the contextual fear-conditioning test. WT, $n = 15$; KO, $n = 15$. (C) Bar graph showing the correct rate in the Y maze spontaneous alteration test. WT, $n = 23$; KO, $n = 22$. (D–G) Analysis of the Morris water maze results of WT and KO mice, including latency traces of the five training days in panel D, latency values in the test in panel E, time in the target quadrant in panel F, and platform crossing times in panel G. WT, $n = 17$; KO, $n = 15$. Two-way ANOVA results in panel D, with differences not significant for each day. (H) Field excitatory postsynaptic potential LTP recording of Schaffer collateral-CA1 synapses. LTP was induced by high-frequency stimulation (HFS; 3 × 100 Hz/s burst times with a 20-second interval). Sample trace scale bar, 0.1 mV and 25 ms. (I) Bar graph showing the average 55 to 60 minutes after HFS relative to the baseline. WT, $n = 7$; KO, $n = 7$. In bar graphs of this figure, dots indicate individual values, and columns with error bars present the mean ± SEM compared with a two-tailed unpaired *t*-test.

or the interspike interval of AP spikes under saturation stimulation (Figure 6N) were comparable between Ctrl and Cre neurons. These data thus demonstrate that deletion of Nr4a1 mostly impairs synaptic AMPAR and NMDAR function but not inhibitory neurotransmission or the intrinsic excitability of CA1 neurons. We further recorded the whole-cell EPSC LTP of Cre-expressing $Nr4a^{fl/fl}$ neurons to verify the contribution of Nr4a1 to synaptic plasticity. Similar to the fEPSP LTP of Nr4a1-KO mice (Figure 3H,I), although Nr4a1-deficient neurons persistently exhibited LTP, the potentiation magnitudes were significantly lower than those of Ctrl neurons (Figure 6O,P).

Next, we examined whether Nr4a1 overexpression could rescue the defects of synaptic transmission and plasticity in Nr4a1-KO mice. We injected $AAV_{Nr4a1\text{-}EGFP}$ into the CA1 region of Nr4a1-KO mice at P0 and recorded synaptic responses 19 to 28 days later (Figure 7A). Expression of Nr4a1 in CA1 PyrNs of Nr4a-KO mice significantly enhanced AMPAR-eEPSCs (Figure 7B,C), while the PPR (Figure 7H) and eIPSCs (Figure 7F,G) were not significantly changed. Intriguingly, NMDAR-eEPSCs were not rescued by Nr4a1 overexpression (Figure 7D,E). The failure to rescue NMDAR functions suggested that Nr4a1 ablation might have caused irreversible NMDAR defects during embryonic development. The magnitudes of LTP were enhanced in Nr4a1-overexpressing neurons (Figure 7I,J). Taken together, Nr4a1 ablation and rescue experiments in single cells verify that Nr4a1 plays an essential role in maintaining excitatory synaptic transmission and plasticity.

3.6 | Nr4a1 binds *Ntrk2* promoter and enhances its expression

To investigate the potential mechanisms by which Nr4a1 modulated excitatory synapses, a chromosome CUT&Tag assay was performed with the isolated mouse hippocampi CA1 tissues. The results showed that Nr4a1 could bind to multiple gene loci involved in classic synaptic plasticity-related signals, including the PI3K-Akt-, neurotrophin-, MAPK- and RAS-related pathways (Figure 8A). *Ntrk2*, the gene encod-

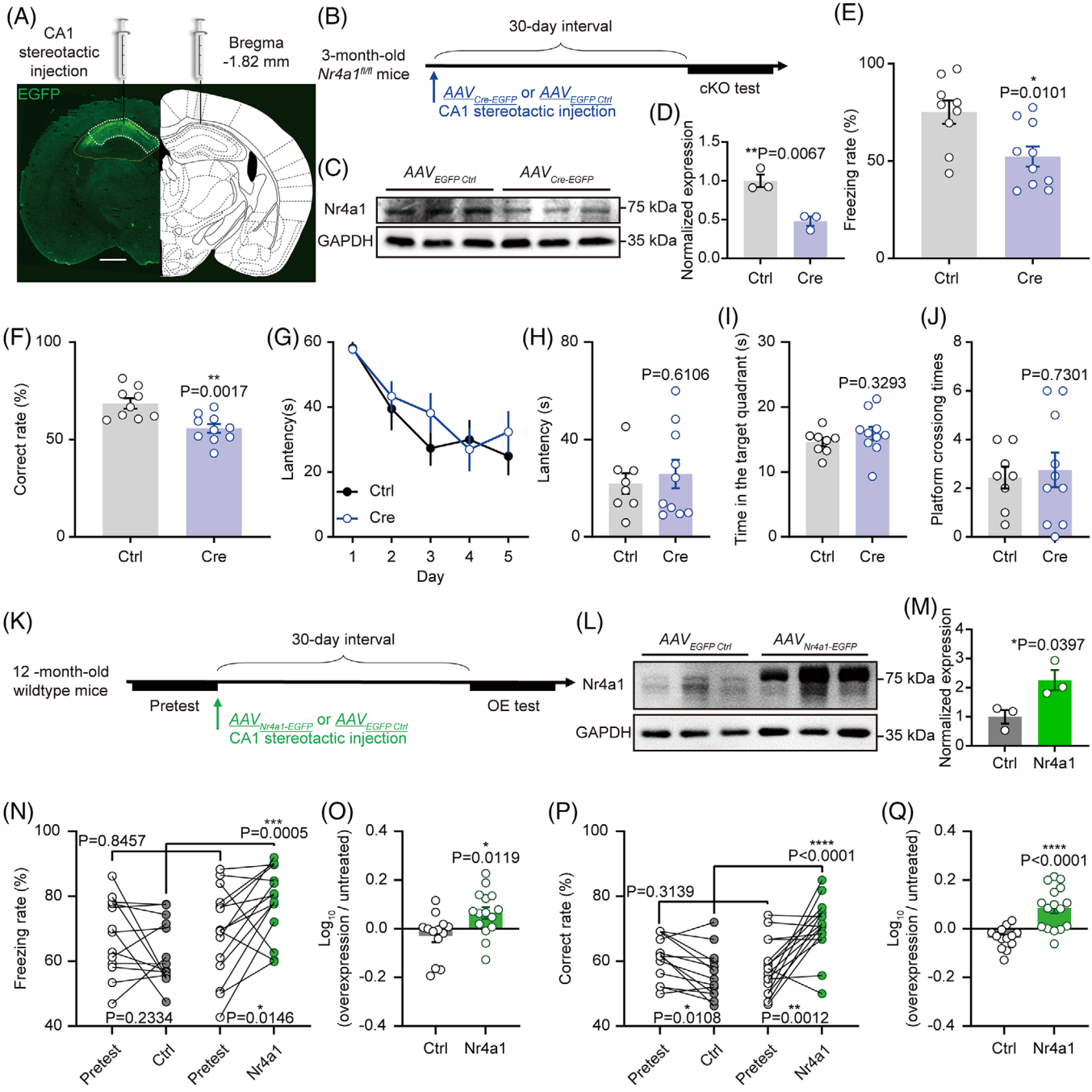

FIGURE 4 Deletion or overexpression of Nr4a1 in hippocampal CA1 pyramidal neuron regulated memory in mice. (A) Stereotactic injection of enhanced green fluorescent protein (EGFP)-tagged adeno-associated virus (AAV) in CA1. Scale bar, 1 mm. (B) Procedure of Nr4a1 CA1 Cre-carrying AAV knockout (cKO) and behavioral tests. (C,D) Protein levels of Nr4a1 in the CA1 of $AAV_{Cre\text{-}EGFP}$ (Cre)- and control $AAV_{EGFP\ Ctrl}$ (Ctrl)-injected mice. (E) Freezing rates of Ctrl and Cre in the contextual fear-conditioning (CFC) test. $n = 9$ to 10 in the Ctrl and Cre groups. (F) Correct rates in the Y maze spontaneous alteration (YM) test. $n = 9$ to 10 in the Ctrl and Cre group. (G–J) Morris water maze test results of Ctrl and Cre mice. Two-way ANOVA used in panel F, nonsignificant results on each day. (K) Procedure of CA1 Nr4a1 overexpression (OE) and behavioral tests. (L,M) Protein levels of Nr4a1 in the CA1 of Ctrl and $AAV_{Nr4a1\text{-}EGFP}$ (Nr4a1)-injected 12-month-old mice. (N–Q) Freezing rates and correct rates of 12-month-old Nr4a1 and Ctrl mice in the CFC (in panels N,O) and the YM (panels P,Q) tests. Lines in panels N and P link the same individual before and after AAV injection. Pretest vs Ctrl, $n = 13$; pretest vs Nr4a1, $n = 15$. *P*-values below the dots present comparisons of the same mouse before and after AAV injection; *P*-values above the connecting lines present the comparisons between Ctrl and Nr4a1- OE group before or after AAV injection. In panels N and P, comparisons between pretests and OE tests were performed by paired *t*-tests, while comparisons between Nr4a1 and Ctrl were performed by two-tailed unpaired *t*-tests. In bar graphs of this figure, dots indicate individual values, and columns with error bars present the mean ± SEM compared with a two-tailed unpaired *t*-test.

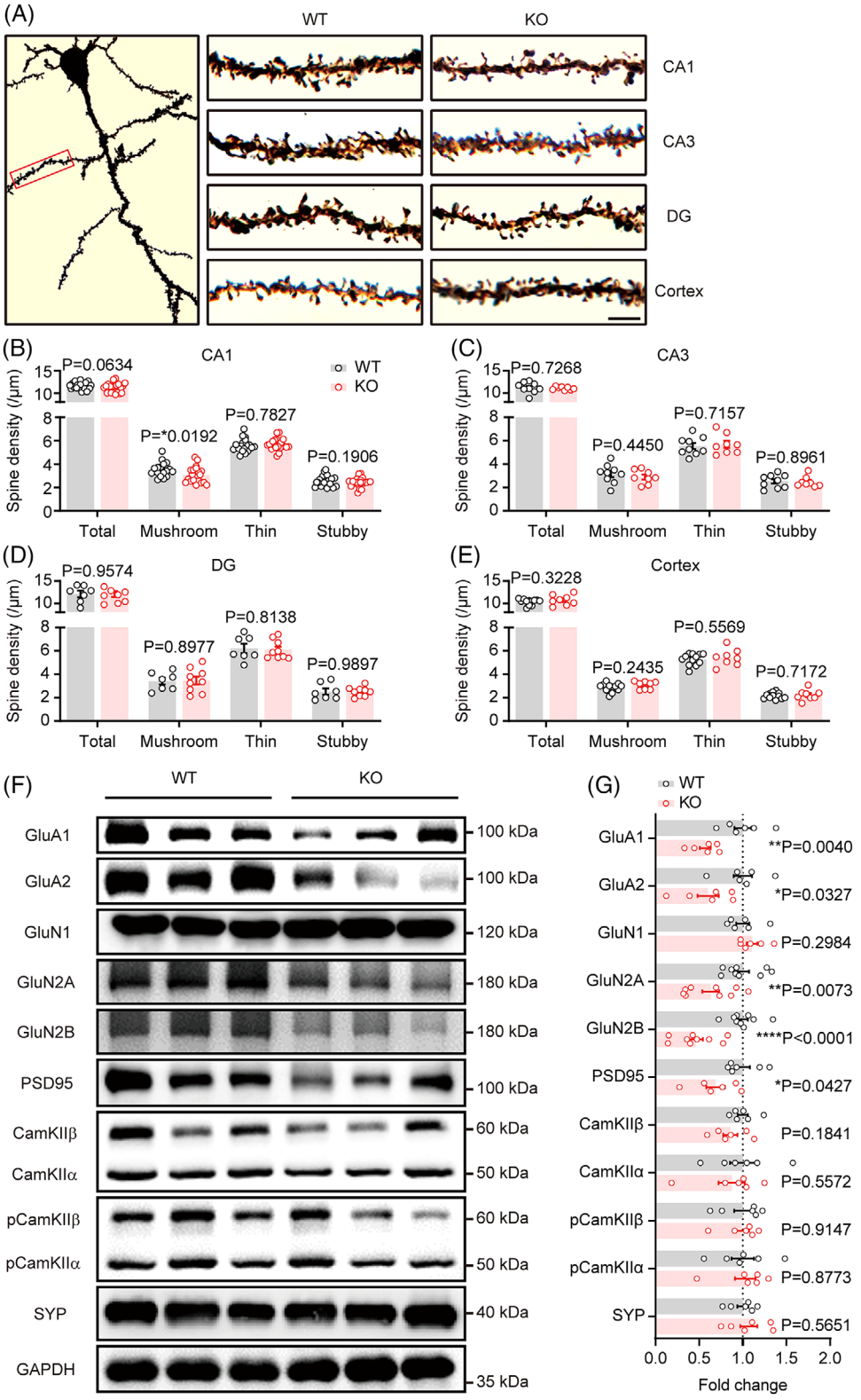

FIGURE 5 Nr4a1 ablation reduced mature dendritic spine density and glutamate receptor expression in CA1 cells. (A) Golgi staining in hippocampal subregions and the cortex in wild type (WT) and knockout (KO) mice. Scale bar = 4 μm. (B–E) Quantitative analysis of the densities of different types of dendritic spines by Golgi staining. Dots indicate individual values, and columns with error bars present the mean ± SEM. $n \geq 6$. Two-tailed unpaired *t*-test. (F) Protein levels of glutamate receptor subunits and some other synaptic transmission/plasticity-related proteins, determined by western blotting. (G) Quantitative analysis of the western blot data in panel F. Dots indicate individual values, and columns with error bars present the mean ± SEM. $n \geq 6$. Two-tailed unpaired *t*-tests.

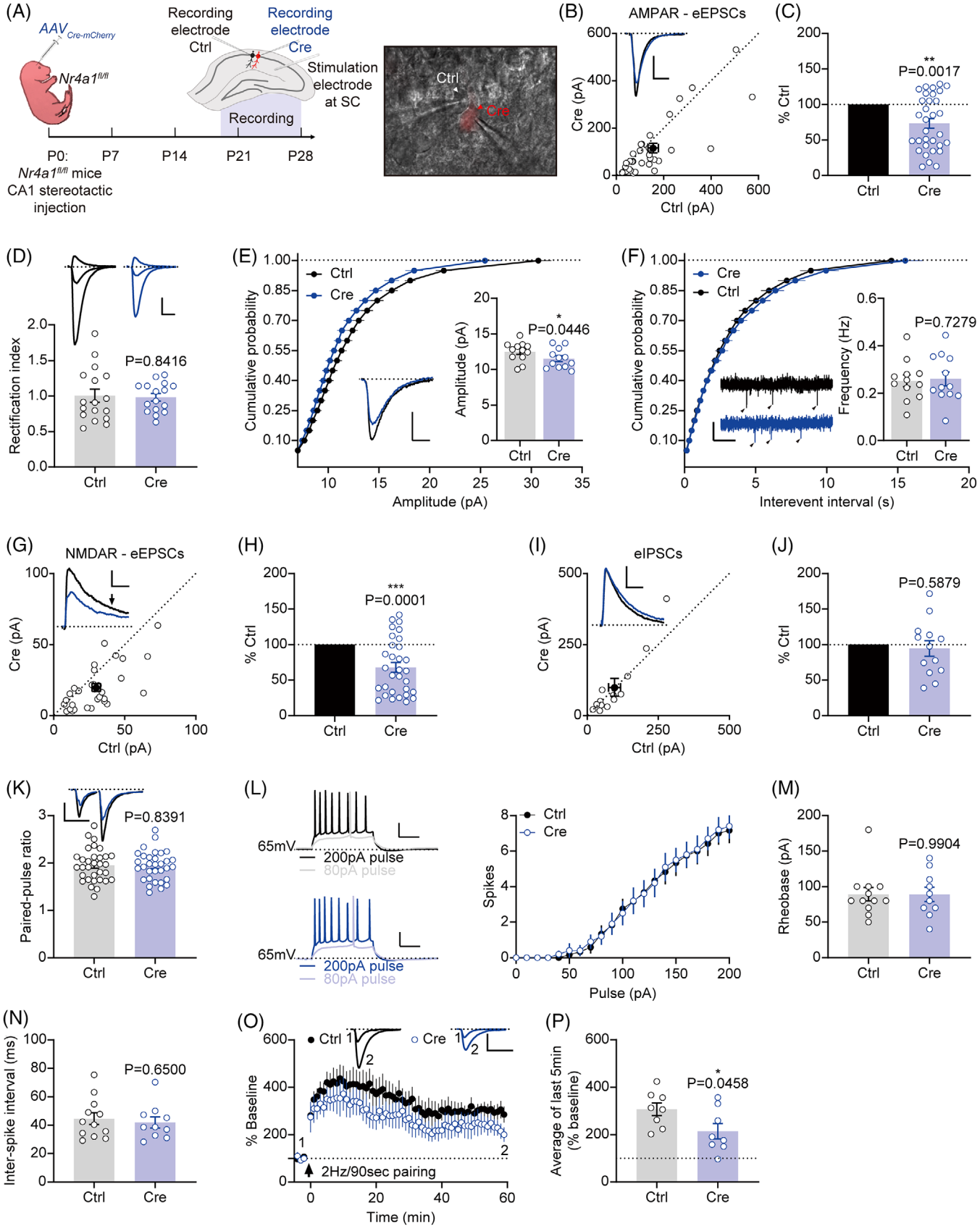

FIGURE 6 Single-cell Nr4a1 deletion in CA1 pyramidal neurons impaired excitatory synaptic transmission and plasticity. (A) Procedure of Nr4a1 Cre-carrying AAV knockout (cKO) and dual-electrode recording. (B) AMPA receptor-evoked excitatory postsynaptic currents (AMPAR-eEPSCs) of adeno-associated virus $(AAV)_{Cre\text{-}mCherry}$-infected neurons (Cre) and neighboring Ctrl neurons (Ctrl). Circles show single dual recordings, and dots with bars show the mean ± SEM. Scale bar, 50 pA and 25 ms. (C) Percentages of Cre relative to Ctrl in panel B. Dots indicate

ing TrkB, was the core and only overlapping gene associated with these pathways (Figure 8A). According to the CUT&Tag results, Nr4a1 mainly bound to the transcription start sites (TSSs) of the target genes (Figure 8B). In *Ntrk2*, Nr4a1 appeared to bind to a segment approximately −2114 to −1794 bp upstream from the ATG initiation codon, which was around the TSS of *Ntrk2* (Figure 8C,D). The ChIP assay of mouse CA1 tissues confirmed the interaction between the *Ntrk2* promoter segment (−2114 to −1794 bp) and Nr4a1 protein (Figure 8E). To examine whether this interaction affected TrkB expression, the mouse *Ntrk2* promoter (−2560 to +2 bp)[34] was fused to the 5′ of the luciferase cDNA, and the transcription was evaluated by the catalytic activity of luciferase expressed in HEK293T cells. Application of mouse Nr4a1 protein enhanced the luciferase activity (Figure 8F). When the Nr4a1-binding segment was deleted (Δ−2114 to −1794), Nr4a1 was unable to change the luciferase activity (Figure 8F). The *Ntrk2* promoter-driven luciferase activity was also tested in N2a cells, a mouse-derived neuroblastoma cell line with endogenous Nr4a1 expression. Knockdown of Nr4a1 with an shRNA (Figure 8G) significantly reduced the luciferase activity driven by full length *Ntrk2* promoter but not by Δ−2114 to −1794 promoter (Figure 8H). The results above demonstrate that the interaction of Nr4a1 with *Ntrk2* promoter at the −2114 to −1794 bp locus enhances the transcription and expression of TrkB.

According to the CUT&Tag assay, we identified four possible Nr4a1-binding motifs at the −2114 to −1794 scale (Figure S6A). The motifs were located at −2020 to −2006 bp (motif 1), −2017 to −2003 bp (motif 2), −1957 to −1937 bp (motif 3), and −1881 to −1866 bp (motif 4) upstream from the ATG initiation codon (Figure S6A). To determine the precise binding position, we constructed *Ntrk2* promoters of which the putative Nr4a1-binding motifs were truncated (Figure S6B). Subsequent luciferase reporter experiments showed that Nr4a1-induced expressing increment of luciferase was almost eliminated under the promoters with motif 1/2 truncation (Δmotif 1/2) and motif 4 truncation (Δmotif 4), which were comparable to the truncation of the whole −2114 to −1794 bp scale (Figure S6C). However, the truncation of motif 3 (Δmotif 3) did not change the Nr4a1 effect to *Ntrk2* promoter-driven luciferase expression (Figure S6C). The result indicates that the binding sites locating at −2020 to −2003 bp (motif 1/2, 5′-AATCATCTCACGTGTCCC-3′) and −1881~−1866 bp (motif 4, 5′-GCAAGGTACGGCAGG-3′) are essential to the Nr4a1 interaction with *Ntrk2* promoter.

Furthermore, we targeted the mouse *Ntrk2* promoter −2114 to −1794 bp segment with CRISPR/Cas9 to confirm the function contribution of the Nr4a1-binding at this locus. An array of three sgRNAs targeting the *Ntrk2* promoter (−2114 to −1794) was designed (Figure S7A) and constructed into an expression vector with Cas9 (Figure S7B). We transfected the N2a cell line with the above TrkB promoter-sgRNAs/Cas9 (CRISPR) vector. Seventy-two hours after the transfection, genomic DNA was collected, and the promoter region of TrkB was cloned into T-vectors (pMD19-T, TAKARA) for Sanger sequencing. In total, nine mutants were identified, and six mutants contained large-fragment deletions (Figure S8C, mutants #1 to #6), while the other three mutants showed several nucleotide indels. We further delivered the CRISPR vector into cultured hippocampal neurons and measured the mEPSCs (Figure S7D). The CRISPR group exhibited remarkable reductions in both amplitude and frequency (Figure S7E,F). The results indicate a crucial role of the Nr4a1-binding segment in *Ntrk2* promoter for synaptic function.

To determine whether NR4A1-dependent regulation of TrkB expression occurred in a human genomic background, a human neuroblastoma cell line, SH-SY5Y, was used. The ChIP assay showed that human NR4A1 could bind to the −2112 to −1961 bp upstream human *NTRK2* initiation codon (Figure S8A,B), which was inside the homologous scale to the Nr4a1-binding −2114 to −1794 bp region of mouse *Ntrk2* promoter. In the luciferase reporter experiment, overexpressing NR4A1 significantly enhanced the *NTRK2* promoter-driven luciferase activity (Figure S8C), indicating that the NR4A1-associated TrkB expressing regulation was available in a human genomic background. Besides, overexpressing NR4A1 in SH-SY5Y increased protein levels of TrkB and functional phosphorylation of downstream Akt, Erk, and CREB (Figure S8D,E). The results demonstrate that the NR4A1-associated TrkB pathway regulation occurs in a human genomic background.

3.7 | Nr4a1 enhances cognition and synaptic transmission through TrkB

Both TrkB mRNA and protein levels were downregulated in CA1 lysates from Nr4a1-KO mice (Figure 8I–K). Consistently, some downstream molecules of the TrkB signaling pathways, including the

individual values, and columns with error bars present the mean ± SEM. $n = 32$ pairs. Nonparametric paired *t*-test. (D) AMPAR rectification index, $n = 17$ pairs, parametric paired *t*-test. Scale bar, 50 pA and 25 ms. (E) The miniature EPSC (mEPSC) amplitude statistics. The line chart with the mean ± SEM dots shows the cumulative probabilities of amplitudes. The bar graph presents the comparison of mean ± SEM. $n = 12$ pairs, parametric paired *t*-test. Scale bar, 5 pA and 10 ms. (F) The mEPSC frequency statistics. Bar graph, $n = 12$ pairs, parametric paired *t*-test. Scale bar, 10 pA and 2 s. (G,H) NMDA receptor (NMDAR)-eEPSCs from dual recordings. NMDAR-eEPSC is the value 150 ms after stimulation (at arrowhead in panel G) when the AMPAR-eEPSC completely vanishes. Scale bar, 25 pA and 50 ms. Panel H, $n = 31$ pairs, nonparametric paired *t*-test. (I,J) Evoked inhibitory postsynaptic currents (eIPSCs) from dual recordings. Scale bar, 50 pA and 50 ms. Panel J, $n = 13$ pairs, nonparametric paired *t*-test. (K) AMPAR-eEPSC paired-pulse ratio, $n = 32$ pairs, parametric paired *t*-test. Scale bar, 100 pA and 50 ms. (L) Input/output curve of action potentials (Aps), with dots presenting the mean ± SEM. Ctrl, $n = 12$; Cre, $n = 10$. Scale bar, 25 mV and 100 ms. (M) Rheobase bar graph. Ctrl, $n = 12$; Cre, $n = 10$. (N) Interspike interval at 200pA-injection. Ctrl, $n = 12$; Cre, $n = 10$. Two-tailed unpaired *t*-test in panels M and N. (O,P) Dual-recorded long-term potentiation. Sample trace, 25 pA and 10 ms. Panel P, average at 55 to 60 minutes after pairing relative to the baseline. Ctrl, $n = 8$; Cre, $n = 8$, two-tailed unpaired *t*-test.

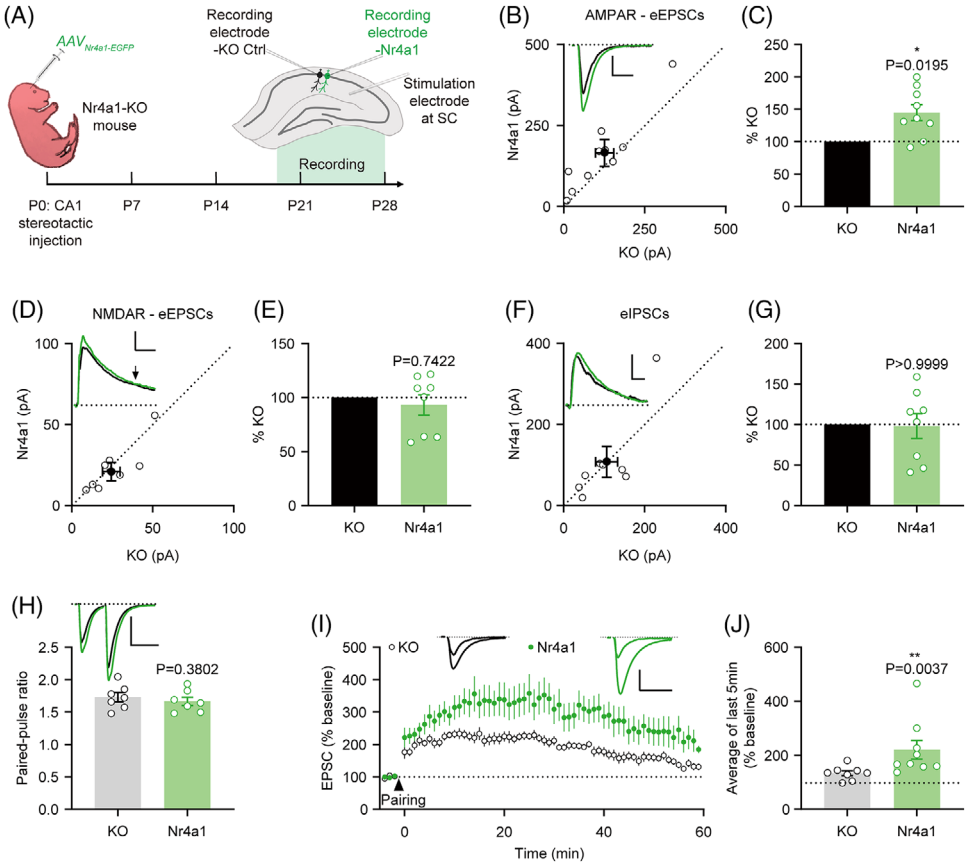

FIGURE 7 Heterogeneous expression of Nr4a1 rescued AMPA receptor-evoked excitatory postsynaptic current (AMPAR-eEPSC) and long-term potentiation (LTP) defects in CA1 pyramidal neurons (PyrNs) of Nr4a1-knockout (KO) mice. (A) The procedure of Nr4a1 CA1 PyrN heterogeneous expression and subsequent dual-electrode whole-cell recording on postnatal days P19 to 28. (B) AMPAR-eEPSCs of adeno-associated virus ($AAV_{Nr4a1\text{-}EGFP}$)-infected neurons (Nr4a1) and neighboring control Nr4a1-KO neurons (KO). Scale bar of sample trace, 50 pA and 25 ms. (C) Bar graph shows the percentage of Nr4a1 to KO. KO and Nr4a1 pairs, $n = 9$, nonparametric paired *t*-test. (D,E) NMDA receptor (NMDAR)-eEPSCs of Nr4a1 and KO. Scale bar of sample trace, 50 pA and 50 ms. KO and Nr4a1 pairs in panel E, $n = 8$, nonparametric paired *t*-test. (F,G) Evoked inhibitory postsynaptic currents (eIPSCs) of KO and Nr4a1 paired recording. Scale bar of sample trace, 25 pA and 25 ms. KO and Nr4a1 pairs in panel G, $n = 8$, nonparametric paired *t*-test. (H) Bar graph of AMPAR-eEPSC paired-pulse ratio of Nr4a1 and KO. Scale bar of sample trace, 200 pA and 50 ms. KO and Nr4a1 pairs, $n = 7$, parametric paired *t*-test. (I,J) LTP of KO and Nr4a1 paired recording. Sample trace scale bar, 50 pA and 50 ms. Panel J, KO, $n = 8$; Nr4a1, $n = 9$, two-tailed unpaired *t*-test. In bar graphs of this figure, dots indicate individual values, and columns with error bars present the mean ± SEM.

phosphorylated forms of Akt, Erk, and cAMP-response element binding (CREB), were also strikingly decreased (Figure 8J,K). To determine whether Nr4a1 enhanced the memory functions in a TrkB-dependent manner, we stereotactically injected $AAV_{Nr4a1\text{-}EGFP}$ or $AAV_{EGFP\ Ctrl}$ to the CA1 region of 12-month-old mice. Then, 16 days later ANA12, a potent TrkB antagonist, was intraperitoneally injected for another 14 days (Figure 8L). ANA12 administration per se did not alter the performance of 12-month-old mice in CFC or YM tests, and Nr4a1 overexpression improved the memory functions of aged mice in both CFC and YM tests (Figure 8M,N). However, ANA12 compromised the Nr4a1-associated cognitive enhancement effects in the CFC and YM tests (Figure 8M,N). ANA12 alone did not change the expressions of Nr4a1 and the TrkB-pathway in the CA1 region, while Nr4a1 overexpression significantly increased the level of TrkB and downstream proteins (Figure 8O,P). However, in Nr4a1 overexpressing CA1 tissues, ANA12 significantly decreased the activation of the TrkB pathway (Figure 8O,P). Consistently, ANA12 administration alone did not affect the AMPAR subunits, NMDAR subunits, or PSD95 expressions in CA1, while Nr4a1 overexpression upregulated GluA1, GluN1, GluN2A/B, and PSD95 (Figure 8Q,R). However, ANA12 diminished the Nr4a1-dependent increase of synaptic proteins (Figure 8Q,R).

To further investigate the critical role of TrkB in Nr4a1-mediated synaptic function improvement, we stereotactically injected TrkB-EGFP encoding LV ($LV_{TrkB\text{-}EGFP}$, TrkB and EGFP were driven by CaMKII promoter and separated with P2A sequence) to P0 Nr4a1-KO mice. Acute hippocampal slices were used to test the synaptic transmission and plasticity of CA1 pyramidal neurons within P19 to P28 (Figure S9A). AMPAR-eEPSC amplitude was mightily elevated in the TrkB-overexpressing neurons, compared to the nearby Nr4a1-KO controls (Figure S9B,C). TrkB overexpression could not change NMDAR-eEPSCs in the Nr4a1-KO neurons (Figure S9D,E), which was consistent with Nr4a1 overexpression (Figure 7D,E). In addition, we did not find

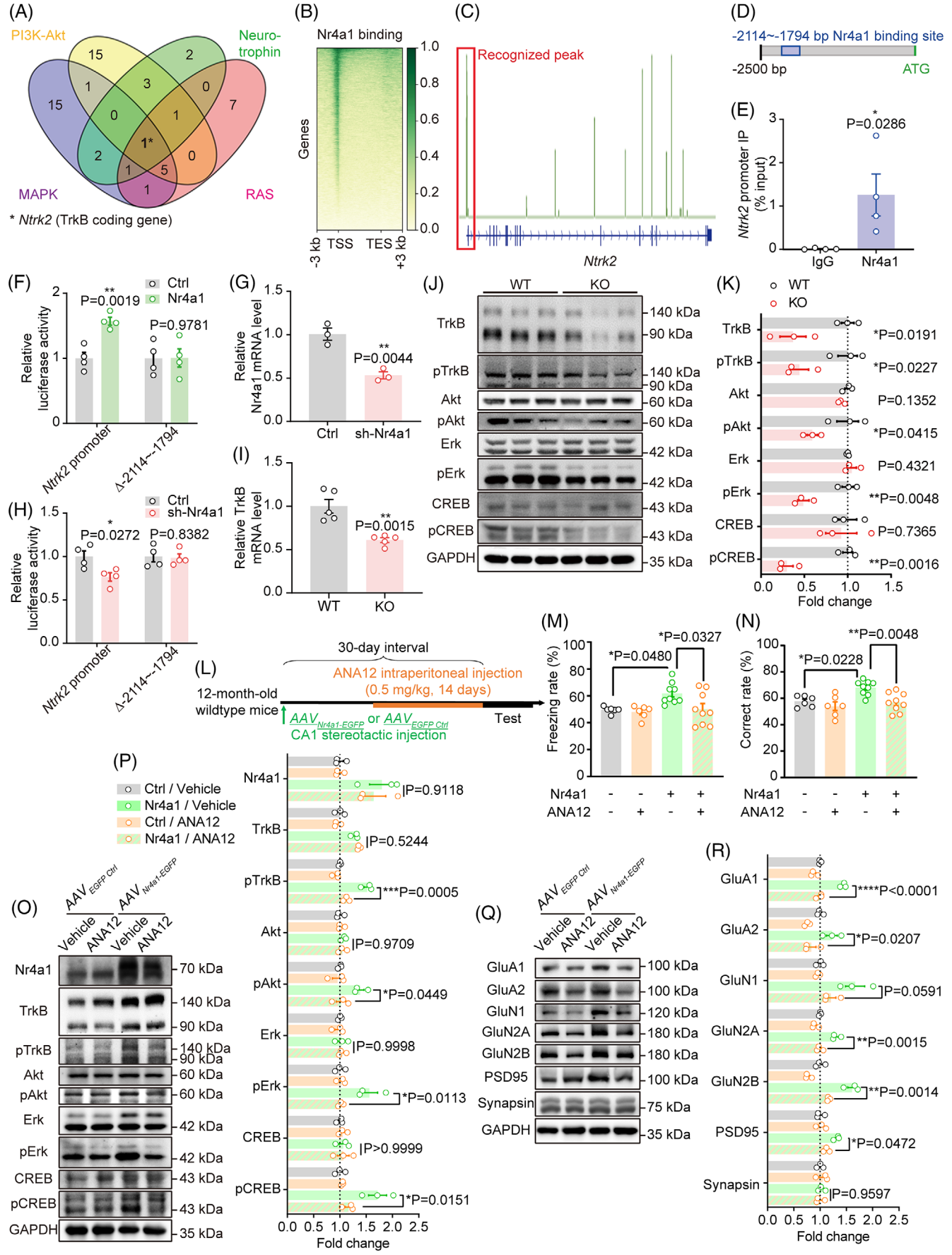
(A)
PI3K-Akt
Neuro-trophin
MAPK
RAS
* Ntrk2 (TrkB coding gene)
(B)
Nr4a1 binding
Genes
-3 kb TSS TES +3 kb
(C)
Recognized peak
Ntrk2
(D)
-2114~-1794 bp Nr4a1 binding site
-2500 bp
ATG
(E)
Ntrk2 promoter IP (% input)
P=0.0286
IgG
Nr4a1
(F)
Relative luciferase activity
Ctrl
Nr4a1
P=0.0019
P=0.9781
Ntrk2 promoter
Δ-2114~-1794
(G)
Relative Nr4a1 mRNA level
P=0.0044
Ctrl
sh-Nr4a1
(H)
Relative luciferase activity
Ctrl
sh-Nr4a1
P=0.0272
P=0.8382
Ntrk2 promoter
Δ-2114~-1794
(I)
Relative TrkB mRNA level
P=0.0015
WT
KO
(J)
WT
KO
TrkB
pTrkB
Akt
pAkt
Erk
pErk
CREB
pCREB
GAPDH
140 kDa
90 kDa
60 kDa
42 kDa
43 kDa
35 kDa
(K)
WT
KO
*P=0.0191
*P=0.0227
P=0.1352
*P=0.0415
P=0.4321
**P=0.0048
P=0.7365
**P=0.0016
Fold change
(L)
30-day interval
ANA12 intraperitoneal injection
(0.5 mg/kg, 14 days)
12-month-old wildtype mice
Test
AAV Nr4a1-EGFP or AAV EGFP Ctrl
CA1 stereotactic injection
(M)
Freezing rate (%)
*P=0.0480
*P=0.0327
Nr4a1
ANA12
(N)
Correct rate (%)
*P=0.0228
**P=0.0048
Nr4a1
ANA12
(O)
AAV EGFP Ctrl
AAV Nr4a1-EGFP
Vehicle
ANA12
Nr4a1
TrkB
pTrkB
Akt
pAkt
Erk
pErk
CREB
pCREB
GAPDH
70 kDa
140 kDa
90 kDa
60 kDa
42 kDa
43 kDa
35 kDa
(P)
Ctrl / Vehicle
Nr4a1 / Vehicle
Ctrl / ANA12
Nr4a1 / ANA12
Nr4a1 P=0.9118
TrkB P=0.5244
pTrkB ***P=0.0005
Akt P=0.9709
pAkt *P=0.0449
Erk P=0.9998
pErk *P=0.0113
CREB P>0.9999
pCREB *P=0.0151
Fold change
(Q)
AAV EGFP Ctrl
AAV Nr4a1-EGFP
Vehicle
ANA12
GluA1
GluA2
GluN1
GluN2A
GluN2B
PSD95
Synapsin
GAPDH
100 kDa
120 kDa
180 kDa
75 kDa
35 kDa
(R)
GluA1 ****P<0.0001
GluA2 *P=0.0207
GluN1 P=0.0591
GluN2A **P=0.0015
GluN2B **P=0.0014
PSD95 *P=0.0472
Synapsin P=0.9597
Fold change

any significant differences in eIPSCs and AMPAR-eEPSC PPR in TrkB-overexpressing neurons compared with Nr4a1-KO controls (Figure S9F–H). Nevertheless, TrkB overexpression enhanced the LTP magnitude in Nr4a1-KO neurons (Figure S9I,J). These electrophysiological results demonstrate the critical role of TrkB in the regulation of Nr4a1 in excitatory synaptic transmission and plasticity.

4 | DISCUSSION

In this study, we showed compelling evidence that an age-dependent Nr4a1 reduction contributes to cognitive decline. In the human population, the NR4A1 expression level in peripheral blood declined with age, especially in older individuals with cognitive impairment. NR4A1 mRNA was also decreased in the human hippocampus with aging. In addition, age-dependent Nr4a1 decline occurred in mice, not only in peripheral blood but also in the hippocampal CA1 region. AAV-mediated Nr4a1-cKO in CA1 impaired cognition in young mice, while Nr4a1 overexpression improved memory functions in old animals. Importantly, eliminating Nr4a1 in CA1 PyrNs reduced the expression of glutamate receptors, impaired excitatory synaptic transmission and LTP, and hampered synaptic maturation. Overexpression of Nr4a1 in CA1 PyrNs rescued synaptic defects in Nr4a1-KO mice. Finally, Nr4a1 bound to the TSS of the *Ntrk2* promoter and enhanced transcription, and improved cognitive and synaptic functions in a TrkB-dependent way.

The Nr4a family is a subset of orphan nuclear receptors that mainly serve as transcription factors. Their role in cognition has recently been studied in rodents. Nr4a1-3 expressions boosted shortly after learning tasks,[16] indicating that they are IEGs during learning. In cognition-impaired aged rats, immediate responses to learning tasks were lost.[14] Contextual fear memory was impaired in young adult transgenic mice expressing Nr4aDN,[16] providing direct evidence that Nr4a deficiency impaired cognition. Consistent with these data, our Nr4a1 knockout mice showed memory impairment at the age of 3 months, suggesting that Nr4a1 is critical to maintaining cognition. Interestingly, the role of Nr4a1 in cognition appeared to rely on its expression in the hippocampal CA1 region. AAV-mediated Nr4a1 deletion in CA1 PryNs impaired contextual fear memory and short-term working memory, which was consistent with the observation from Nr4a1-KO mice. Moreover, overexpressing Nr4a1 in CA1 improved the performance of old mice in different cognition tests (CFC and YM tests in this study and object location memory test in the study of Kwapis et al.[14]).

In this study, we found an age-dependent decline in Nr4a1 in the mouse hippocampus. A recent study also identified that Nr4a1 was reduced in the brains of old mice using single-cell transcriptomic

FIGURE 8 Nr4a1 enhanced tyrosine kinase receptor B (TrkB) expression via directly binding to the −2114 to −1794 bp promoter of *Ntrk2*. (A) Venn diagram of Nr4a1-binding genes related to synaptic transmission and plasticity pathways. (B) Nr4a1 gene-biding pattern. Nr4a1 dominantly binds to the transcription start site (TSS) rather than the transcription end site (TES). (C) Nr4a1 binding signals at the full length *Ntrk2* gene locus. The recognized signal peak was near the TSS. (D) Predicted Nr4a1 binding site at the *Ntrk2* promoter. (E) Chromatin immunoprecipitation (ChIP) analysis was performed to assess the interaction of Nr4a1 and the *Ntrk2* promoter. $n = 4$ per group, two-tailed unpaired *t*-test. (F) Luciferase activity in HEK293T cells. $n = 4$ per group. Two-tailed unpaired *t*-test. (G) Nr4a1 mRNA levels in shRNA-based Nr4a1 knockdown (sh-Nr4a1) N2a cell lines and Ctrl cells. $n = 3$, two-tailed unpaired *t*-test. (H) Luciferase activity in control naïve and Nr4a1 knockdown N2a cells from panel G. $n = 4$ per group. Two-tailed unpaired *t*-test. (I) mRNA level of TrkB examined by quantitative polymerase chain reaction (qPCR) in CA1. $n = 5$ per group, two-tailed unpaired *t*-test. (J,K) Protein level of the TrkB pathway in CA1 from wild type (WT) and Nr4a1-knockout (KO) mice. $n = 3$, two-tailed unpaired *t*-test. (L) Procedure of CA1 Nr4a1 overexpression and ANA12 administration in 12-month-old mice and behavioral tests. (M) Bar graph of the freezing rate in the contextual fear conditioning test for the 12-month-old mice with Nr4a1 overexpression/ANA12 administration. $Nr4a1^{-}/ANA12^{-}$ vs $Nr4a1^{-}/ANA12^{+}$, $P = 0.9869$; $Nr4a1^{-}/ANA12^{-}$ vs $Nr4a1^{+}/ANA12^{-}$, $P = *0.0480$; $Nr4a1^{-}/ANA12^{-}$ vs $Nr4a1^{+}/ANA12^{+}$, $P = 0.9991$; $Nr4a1^{-}/ANA12^{+}$ vs $Nr4a1^{+}/ANA12^{-}$, $P = *0.0210$; $Nr4a1^{-}/ANA12^{+}$ vs $Nr4a1^{+}/ANA12^{+}$, $P = 0.9577$; $Nr4a1^{+}/ANA12^{-}$ vs $Nr4a1^{+}/ANA12^{+}$, $P = *0.0327$. (N) Bar graph of the correct rate in the Y maze spontaneous alteration test for the mice with Nr4a1 overexpression/ANA12 administration. $Nr4a1^{-}/ANA12^{-}$ vs $Nr4a1^{-}/ANA12^{+}$, $P = 0.7491$; $Nr4a1^{-}/ANA12^{-}$ vs $Nr4a1^{+}/ANA12^{-}$, $*P = 0.0228$; $Nr4a1^{-}/ANA12^{-}$ vs $Nr4a1^{+}/ANA12^{+}$, $P = 0.9944$; $Nr4a1^{-}/ANA12^{+}$ vs $Nr4a1^{+}/ANA12^{-}$, $P = **0.0015$; $Nr4a1^{-}/ANA12^{+}$ vs $Nr4a1^{+}/ANA12^{+}$, $P = 0.8305$; $Nr4a1^{+}/ANA12^{-}$ vs $Nr4a1^{+}/ANA12^{+}$, $P = **0.0048$. In panels M and N, $Nr4a1^{-}/ANA12^{-}$, $n = 6$; $Nr4a1^{-}/ANA12^{+}$, $n = 6$; $Nr4a1^{+}/ANA12^{-}$, $n = 9$; $Nr4a1^{+}/ANA12^{+}$, $n = 9$, one-way ANOVA. (O,P) Protein level of the TrkB pathway molecules in CA1 from the 12-month-old mice with Nr4a1 overexpression/ANA12 administration. $n = 3$. $Nr4a1^{-}/ANA12^{-}$ vs $Nr4a1^{-}/ANA12^{+}$, $Nr4a1^{-}/ANA12^{-}$ vs $Nr4a1^{+}/ANA12^{-}$, $Nr4a1^{-}/ANA12^{-}$ vs $Nr4a1^{+}/ANA12^{+}$, $Nr4a1^{-}/ANA12^{+}$ vs $Nr4a1^{+}/ANA12^{-}$, $Nr4a1^{-}/ANA12^{+}$ vs $Nr4a1^{+}/ANA12^{+}$ and $Nr4a1^{+}/ANA12^{-}$ vs $Nr4a1^{+}/ANA12^{+}$, respectively, in Nr4a1 $P > 0.9999$, $P = 0.0418$ (*), 0.1048, 0.0392 (*), 0.0983 and 0.9118; in TrkB $P = 0.8028$, 0.0043 (**), 0.0009 (***), 0.0015 (**), 0.0004 (***) and 0.5244; in pTrkB $P = 0.5623$, < 0.0001 (****), 0.2153, < 0.0001 (****), 0.0329 (*), and 0.0005 (***); in Akt $P = 0.9746$, 0.6152, 0.8451, 0.8356, 0.9764, and 0.9709; in pAkt $P = 0.9761$, 0.0338 (*), 0.9968, 0.0194 (*), 0.9269 and 0.0449 (*); in Erk $P = 0.9665$, 0.9657, 0.9450, 0.7970, 0.7523, and 0.9998; in pErk $P = 0.9967$, 0.0094 (**), 0.9989, 0.0123 (*), 0.9999, and 0.0113 (*); in CREB $P = 0.9494$, 0.9274, 0.9269, 0.9998, 0.9998 and > 0.9999; in pCREB $P = 0.9865$, 0.0033 (**), 0.6416, 0.0049 (**), 0.8192, and 0.0151 (*). One-way ANOVA in panel P. (Q,R) Protein level of some glutamate receptor subunits, postsynaptic density 95 (PSD95) and synapsin in CA1 from the 12-month-old mice with Nr4a1 overexpression/ANA12 administration. $n = 3$. $Nr4a1^{-}/ANA12^{-}$ vs $Nr4a1^{-}/ANA12^{+}$, $Nr4a1^{-}/ANA12^{-}$ vs $Nr4a1^{+}/ANA12^{-}$, $Nr4a1^{-}/ANA12^{-}$ vs $Nr4a1^{+}/ANA12^{+}$, $Nr4a1^{-}/ANA12^{+}$ vs $Nr4a1^{+}/ANA12^{-}$, $Nr4a1^{-}/ANA12^{+}$ vs $Nr4a1^{+}/ANA12^{+}$ and $Nr4a1^{+}/ANA12^{-}$ vs $Nr4a1^{+}/ANA12^{+}$, respectively, in GluA1 $P = 0.1064$, < 0.0001 (****), 0.9936, < 0.0001 (****), 0.1521, and < 0.0001 (****); in GluA2 $P = 0.1636$, 0.2054, 0.4064, 0.0081 (**), 0.8909, and 0.0207 (*); in GluN1 0.9910, 0.0092 (**), 0.5523, 0.0064 (**), 0.4048, and 0.0591; in GluN2A $P = 0.5930$, 0.0018(**), > 0.9999, 0.0003 (***), 0.7447, and 0.0015 (**); in GluN2B $P = 0.0626$, 0.0002 (***), 0.2149, < 0.0001 (****), 0.0036 (**), and 0.0014 (**); in PSD95 $P = 0.9871$, 0.0034 (**), 0.2602, 0.0050 (**), 0.3898, and 0.0472 (*). One-way ANOVA in panel R. In bar graphs of this figure, dots indicate individual values, and columns with error bars present the mean ± SEM.

analysis.[35] In addition, we found that Nr4a1/NR4A1 also decreased with aging in the PBMCs of mice and humans. NR4A1 expression was further decreased in patients with AD and Parkinson's disease (PD)[36] and individuals with cognitive disorders, indicating that NR4A1 in blood might serve as a potential early-diagnosis target for neurodegeneration.

Aging-related cognitive impairment involves synaptic alterations in the hippocampal CA1 region in rats.[37] The dendritic spines, especially the mature mushroom-type spine, of CA1 PyrNs gradually become sparser with aging.[38] We observed that Nr4a1-KO reduced mature mushroom-type spines even in 3-month-old mice, suggesting that age-dependent impairment in spines might at least partially be caused by the Nr4a1 reduction. Aging also causes reductions in AMPAR and NMDAR in the hippocampus.[39,40] In the current study, glutamate receptor subunits, including GluA1, GluA2, GluN2A, and GluN2B, were significantly reduced in CA1 lysates in young Nr4a1-KO mice, indicating the attenuation of excitatory synaptic transmission. Consistent with conformational and molecular changes, electrophysiological analysis demonstrated that both AMPAR- and NMDAR-mediated EPSCs were suppressed in Nr4a1-deleted neurons, while presynaptic neurotransmitter release was unaffected. Furthermore, ablation of Nr4a1 did not alter IPSCs, suggesting that Nr4a1 deletion predominantly impaired the postsynaptic portion of excitatory transmission.

NMDA and AMPA receptors play pivotal roles in the expression and maintenance of synaptic plasticity, through which NMDAR is in charge of LTP induction, while AMPAR trafficking to postsynaptic membrane mediates the synaptic potentiation.[9,41–43] In line with the suppression of AMPAR and NMDAR, we observed the attenuation of LTP Nr4a1-deleted CA1 PyrNs. Interestingly, it has been reported that Nr4aDN transgenic diminished the late-phase (≈3 hours) of LTP which was transcription-dependent,[44,45] suggesting that the transcription factor function of Nr4a1 had a direct effect on LTP. Taken together, these findings indicate that Nr4a1 decline contributes to age-related cognitive impairment through damage to excitatory synaptic conformation and concomitant impairments in synaptic transmission and plasticity.

Nr4a gene expression is regulated by certain signaling pathways. In a PD model, α-synuclein induced diseases by inhibiting the NF-κB/Nr4a1 signaling pathway.[46] Learning-induced Nr4a expression required the interaction between CREB and the histone acetyltransferase CBP, and the *Nr4a* promoter had a domain on which both proteins could act.[16,47] In addition, HDAC3 repressed Nr4a1/2 and, as a result, contributed to memory impairment in cognition-impaired old mice.[14]

The downstream molecular mechanism by which Nr4a regulates cognition, however, is poorly understood. Here, using CUT&Tag assay, we identified that Nr4a1 bound to the promoter of TrkB, which is the intersection among these synaptic plasticity-related pathways. Nr4a1 bound to the −2114 to −1794 region of the *Ntrk2* promoter and enhanced its expression. The NR4A1-induced TrkB-expressing regulation was also applied to human genomic background. Pharmacologically blocking TrkB with ANA12 compromised Nr4a1 overexpression-induced cognitive enhancement of aged mice. Further, single-cell heterogeneously expressing TrkB rescued the AMPR-mediated synaptic transmission and plasticity in Nr4a1-KO CA1 pyramidal neurons. The results suggest that TrkB is critical to the Nr4a1 modulation in cognition. In the prevailing view, TrkB signaling plays a pivotal role in synaptic plasticity and memory function, and TrkB deletion decreases the spine densities of CA1 PyrNs in aged mice.[48] Chemical activation of TrkB rescued long-term synaptic plasticity in the hippocampus of aged rats and ameliorated spatial memory deficits by enhancing spine growth and LTP in an AD mouse model.[49] TrkB functions in regulating excitatory neurotransmission have been well studied in the BDNF/TrkB/CREB axis, one of the most widespread consensus mechanisms in synaptic plasticity.[50] BDNF, a ligand of TrkB, binds and activates TrkB, promoting NMDAR trafficking into synapses.[51] Activated TrkB can enhance the expression of GluN2A/2B subunits of NMDARs and GluA1/2 subunits of AMPARs.[18,52] Therefore, TrkB is very likely one of the major players mediating Nr4a1-dependent regulation of spine conformation and excitatory synaptic function, as well as cognition.

In summary, we showed that Nr4a1 was an important factor in maintaining normal cognition with age and positively regulates TrkB expression through direct promoter binding. The findings profile a probable molecular target for the early diagnosis and treatment of age-related cognitive impairment.

AUTHOR CONTRIBUTIONS

Yun Xu conceived the study. Jiang Chen, Zhi Zhang, Ying Liu, Yun Stone Shi, Lili Huang, Yi Liu, Dan Yang, Pinyi Liu, Qingqing Li, Xin Shu, and Lushan Xu performed most of the experiments and data analysis. Xinyu Bao performed in vitro cell culture. Jiang Chen, Zhi Zhang, and Xiaolei Zhu wrote the first version of the manuscript. Yun Xu, Xiaolei Zhu, and Yun Stone Shi revised the manuscript. All the authors approved the final version.

ACKNOWLEDGMENTS

We gratefully acknowledge all the participants involved in this work for their dedication. This research was supported by the National Natural Science Foundation of China (81920108017, 82130036, 81630028 to Y.X., 81971009 to X.Z., 82271891, 81901161 to J.C.), the National Science and Technology Innovation 2030 – Major Program of Brain Science and Brain-Like Researches (2022ZD0211800 to Y.X.), the Jiangsu Province Key Medical Discipline (ZDXKA2016020 to Y.X.), the Natural Science Foundation of Jiangsu Province (BK20231120 to X.Z.), and the Nanjing Medical Science and Technology Development Foundation (ZKX22025 to X.Z.).

CONFLICT OF INTEREST STATEMENT

The authors declare no conflicts of interest.

ORCID

Xiaolei Zhu https://orcid.org/0000-0003-4696-9696

REFERENCES

1. Langa KM, Levine DA. The diagnosis and management of mild cognitive impairment: a clinical review. *JAMA*. 2014;312(23):2551-2561.

2. Park DC, Reuter-Lorenz P. The adaptive brain: aging and neurocognitive scaffolding. *Annu Rev Psychol*. 2009;60:173-196.
3. Saez-Atienzar S, Masliah E. Cellular senescence and Alzheimer disease: the egg and the chicken scenario. *Nat Rev Neurosci*. 2020;21(8):433-444.
4. Satoh A, Imai SI, Guarente L. The brain, sirtuins, and ageing. *Nat Rev Neurosci*. 2017;18(6):362-374.
5. Xue Z, Ye L, Ge J, et al. Wwl70-induced ABHD6 inhibition attenuates memory deficits and pathological phenotypes in APPswe/PS1dE9 mice. *Pharmacol Res*. 2023:106864.
6. Lu J, Li D, Li F, et al. Montreal cognitive assessment in detecting cognitive impairment in Chinese elderly individuals: a population-based study. *J Geriatr Psychiatry Neurol*. 2011;24(4):184-190.
7. Neves G, Cooke SF, Bliss TV. Synaptic plasticity, memory and the hippocampus: a neural network approach to causality. *Nat Rev Neurosci*. 2008;9(1):65-75.
8. Burke SN, Barnes CA. Neural plasticity in the ageing brain. *Nat Rev Neurosci*. 2006;7(1):30-40.
9. Herring BE, Nicoll RA. Long-term potentiation: from CaMKII to AMPA receptor trafficking. *Annu Rev Physiol*. 2016;78:351-365.
10. Ramachandran B, Ahmed S, Zafar N, Dean C. Ethanol inhibits long-term potentiation in hippocampal CA1 neurons, irrespective of lamina and stimulus strength, through neurosteroidogenesis. *Hippocampus*. 2015;25(1):106-118.
11. Ge J, Xue Z, Shu S, et al. MiR-431 attenuates synaptic plasticity and memory deficits in APPswe/PS1dE9 mice. *JCI Insight*. 2023;8(12):e166270.
12. Herring JA, Elison WS, Tessem JS. Function of Nr4a orphan nuclear receptors in proliferation. *Apoptosis and Fuel Utilization Across Tissues Cells*. 2019;8(11):1373.
13. von Hertzen LS, Giese KP. Memory reconsolidation engages only a subset of immediate-early genes induced during consolidation. *J Neurosci*. 2005;25(8):1935-1942.
14. Kwapis JL, Alaghband Y, López AJ, et al. HDAC3-Mediated repression of the Nr4a family contributes to age-related impairments in long-term memory. *J Neurosci*. 2019;39(25):4999-5009.
15. Pena de Ortiz S, Maldonado-Vlaar CS, Carrasquillo Y. Hippocampal expression of the orphan nuclear receptor gene hzf-3/nurr1 during spatial discrimination learning. *Neurobiol Learn Mem*. 2000;74(2):161-178.
16. Hawk JD, Bookout AL, Poplawski SG, et al. NR4A nuclear receptors support memory enhancement by histone deacetylase inhibitors. *J Clin Invest*. 2012;122(10):3593-3602.
17. Lai KO, Wong AS, Cheung MC, et al. TrkB phosphorylation by Cdk5 is required for activity-dependent structural plasticity and spatial memory. *Nat Neurosci*. 2012;15(11):1506-1515.
18. Caldeira MV, Melo CV, Pereira DB, et al. Brain-derived neurotrophic factor regulates the expression and synaptic delivery of alpha-amino-3-hydroxy-5-methyl-4-isoxazole propionic acid receptor subunits in hippocampal neurons. *J Biol Chem*. 2007;282(17):12619-12628.
19. Huang L, Chen X, Sun W, et al. Early Segmental white matter fascicle microstructural damage predicts the corresponding cognitive domain impairment in cerebral small vessel disease patients by automated fiber quantification. *Front Aging Neurosci*. 2020;12:598242.
20. Zhang X, Zhu XL, Ji BY, et al. LncRNA-1810034E14Rik reduces microglia activation in experimental ischemic stroke. *J Neuroinflammation*. 2019;16(1):75.
21. Liu Y, Bian H, Xu S, et al. Muscone ameliorates synaptic dysfunction and cognitive deficits in APP/PS1 mice. *J Alzheimers Dis*. 2020;76(2):491-504.
22. Tao W, Yu L, Shu S, et al. miR-204-3p/Nox4 mediates memory deficits in a mouse model of Alzheimer's disease. *Mol Ther*. 2021;29(1):396-408.
23. Chen J, Jin J, Zhang X, et al. Microglial lnc-U90926 facilitates neutrophil infiltration in ischemic stroke via MDH2/CXCL2 axis. *Mol Ther*. 2021;29(9):2873-2885.
24. Yang Y, Chen J, Chen X, et al. Endophilin A1 drives acute structural plasticity of dendritic spines in response to Ca2+/calmodulin. *J Cell Biol*. 2021;220(6).
25. Ancona Esselmann SG, Diaz-Alonso J, Levy JM, Bemben MA, Nicoll RA. Synaptic homeostasis requires the membrane-proximal carboxy tail of GluA2. *Proc Natl Acad Sci U S A*. 2017;114(50):13266-13271.
26. Granger AJ, Shi Y, Lu W, Cerpas M, Nicoll RA. LTP requires a reserve pool of glutamate receptors independent of subunit type. *Nature*. 2013;493(7433):495-500.
27. Stemmer M, Thumberger T, Del Sol Keyer M, Wittbrodt J, Mateo JL. CCTop: an intuitive, flexible and reliable CRISPR/Cas9 target prediction tool. *PLoS One*. 2015;10(4):e0124633.
28. Chen J, Shu S, Chen Y, et al. AIM2 deletion promotes neuroplasticity and spatial memory of mice. *Brain Res Bull*. 2019;152:85-94.
29. Kaya-Okur HS, Wu SJ, Codomo CA, et al. CUT&Tag for efficient epigenomic profiling of small samples and single cells. *Nat Commun*. 2019;10(1):1930.
30. McEwen BS, Milner TA. Understanding the broad influence of sex hormones and sex differences in the brain. *J Neurosci Res*. 2017;95(1-2):24-39.
31. Bronikowski AM, Meisel RP, Biga PR, et al. Sex-specific aging in animals: perspective and future directions. *Aging Cell*. 2022;21(2):e13542.
32. Kang HJ, Kawasawa YI, Cheng F, et al. Spatio-temporal transcriptome of the human brain. *Nature*. 2011;478(7370):483-489.
33. Lu W, Shi Y, Jackson AC, et al. Subunit composition of synaptic AMPA receptors revealed by a single-cell genetic approach. *Neuron*. 2009;62(2):254-268.
34. Kingsbury TJ, Murray PD, Bambrick LL, Krueger BK. Ca(2+)-dependent regulation of TrkB expression in neurons. *J Biol Chem*. 2003;278(42):40744-40748.
35. Ximerakis M, Lipnick SL, Innes BT, et al. Single-cell transcriptomic profiling of the aging mouse brain. *Nat Neurosci*. 2019;22(10):1696-1708.
36. Montarolo F, Perga S, Martire S, et al. Altered NR4A subfamily gene expression level in peripheral blood of parkinson's and Alzheimer's disease patients. *Neurotox Res*. 2016;30(3):338-344.
37. Shetty MS, Sharma M, Sajikumar S. Chelation of hippocampal zinc enhances long-term potentiation and synaptic tagging/capture in CA1 pyramidal neurons of aged rats: implications to aging and memory. *Aging Cell*. 2017;16(1):136-148.
38. von Bohlen und Halbach O, Zacher C, Gass P, Unsicker K. Age-related alterations in hippocampal spines and deficiencies in spatial memory in mice. *J Neurosci Res*. 2006;83(4):525-531.
39. Morrison JH, Baxter MG. The ageing cortical synapse: hallmarks and implications for cognitive decline. *Nat Rev Neurosci*. 2012;13(4):240-250.
40. Shi L, Adams MM, Linville MC, et al. Caloric restriction eliminates the aging-related decline in NMDA and AMPA receptor subunits in the rat hippocampus and induces homeostasis. *Exp Neurol*. 2007;206(1):70-79.
41. Ben-Ari Y, Aniksztejn L, Bregestovski P. Protein kinase C modulation of NMDA currents: an important link for LTP induction. *Trends Neurosci*. 1992;15(9):333-339.
42. Diering GH, Huganir RL. The AMPA Receptor Code of Synaptic Plasticity. *Neuron*. 2018;100(2):314-329.
43. Jiang CH, Wei M, Zhang C, Shi YS. The amino-terminal domain of GluA1 mediates LTP maintenance via interaction with neuroplastin-65. *Proc Natl Acad Sci USA*. 2021;118(9).
44. Bridi MS, Abel T. The NR4A orphan nuclear receptors mediate transcription-dependent hippocampal synaptic plasticity. *Neurobiol Learn Mem*. 2013;105:151-158.

45. Bridi MS, Hawk JD, Chatterjee S, Safe S, Abel T. Pharmacological activators of the NR4A nuclear receptors enhance LTP in a CREB/CBP-dependent manner. *Neuropsychopharmacology*. 2017;42(6):1243-1253.
46. Jia C, Qi H, Cheng C, et al. α-Synuclein Negatively Regulates Nurr1 Expression Through NF-κB-Related Mechanism. *Front Mol Neurosci*. 2020;13:64.
47. Vecsey CG, Hawk JD, Lattal KM, et al. Histone deacetylase inhibitors enhance memory and synaptic plasticity via CREB:cBP-dependent transcriptional activation. *J Neurosci*. 2007;27(23):6128-6140.
48. von Bohlen und Halbach O, Minichiello L, Unsicker K. TrkB but not trkC receptors are necessary for postnatal maintenance of hippocampal spines. *Neurobiol Aging*. 2008;29(8):1247-1255.
49. Wang S, Yao H, Xu Y, et al. Therapeutic potential of a TrkB agonistic antibody for Alzheimer's disease. *Theranostics*. 2020;10(15):6854-6874.
50. Minichiello L. TrkB signalling pathways in LTP and learning. *Nat Rev Neurosci*. 2009;10(12):850-860.
51. Suen PC, Wu K, Levine ES, et al. Brain-derived neurotrophic factor rapidly enhances phosphorylation of the postsynaptic N-methyl-D-aspartate receptor subunit 1. *Proc Natl Acad Sci USA*. 1997;94(15):8191-8195.
52. Caldeira MV, Melo CV, Pereira DB, Carvalho RF, Carvalho AL, Duarte CB. BDNF regulates the expression and traffic of NMDA receptors in cultured hippocampal neurons. *Mol Cell Neurosci*. 2007;35(2):208-219.

SUPPORTING INFORMATION

Additional supporting information can be found online in the Supporting Information section at the end of this article.

How to cite this article: Chen J, Zhang Z, Liu Y, et al. Progressive reduction of nuclear receptor Nr4a1 mediates age-dependent cognitive decline. *Alzheimer's Dement*. 2024;20:3504–3524. https://doi.org/10.1002/alz.13819